

# Systematic Effects on the Genus Topology of Large Scale Structure of the Universe

Young-Rae Kim<sup>1</sup>, Yun-Young Choi<sup>2</sup>, Sungsoo S. Kim<sup>3</sup>, Kap-Sung Kim<sup>2</sup>, Jeong-Eun Lee<sup>3</sup>,  
Jihye Shin<sup>3</sup>, and Minbae Kim<sup>3</sup>

<sup>1</sup>*School of Physics, Korea Institute for Advanced Study, Heogiro 85, Seoul 130-722, Korea*

<sup>2</sup>*Department of Astronomy and Space Science, Kyung Hee University, Gyeonggi 446-701, Korea*

<sup>3</sup>*School of Space Research, Kyung Hee University, Gyeonggi 446-701, Korea*

## ABSTRACT

Large-scale structure of the universe is a useful cosmological probe of the primordial non-Gaussianity and the expansion history of the universe because its topology does not change with time in the linear regime in the standard paradigm of structure formation. However, when the topology of iso-density contour surfaces is measured from an observational data, many systematic effects are introduced due to the finite size of pixels used to define the density field, non-linear gravitational evolution, redshift-space distortion, shot noise (discrete sampling), and bias in the distribution of the density field tracers. We study the various systematic effects on the genus curve to a great accuracy by using the Horizon Run 2 simulation of a  $\Lambda$ CDM cosmology. We numerically measure the genus curve from the gravitationally evolved matter and dark matter halo density fields. It is found that all the non-Gaussian deviations due to the systematic effects can be modeled by using a few low-order Hermite polynomials from  $H_0$  to  $H_4$ . We compare our results with the analytic theories whenever possible, and find many new terms in the Hermite series that are making significant contributions to the non-Gaussian deviations. In particular, it is found that the amplitude drop of the genus curve due to the non-linear gravitational evolution can be accurately modeled by two terms  $H_0$  and  $H_2$  with coefficients both proportional to  $\sigma_0^2$ , the mean-square density fluctuation.

*Subject headings:* large-scale structure of universe – cosmology: observations, method: numerical

## 1. Introduction

The topology of large-scale structures (LSS) of the universe has long been used as a probe of non-Gaussianity of the primordial density fluctuations (Gott et al. 1986; Matsubara 1994; Park et al. 2005; Hikage et al. 2006; Hikage et al. 2008). It has also been recently suggested to use the LSS topology as a cosmological invariant that can be used to reconstruct the expansion history of the universe (Park & Kim 2010; Zunckel et al. 2011; Wang et al. 2012; Blake et al. 2013; Speare et al. 2013). The cosmological genus statistic has been the most popular measure of the LSS topology and used to constrain the primordial non-Gaussianity (Choi et al. 2013), galaxy formation mechanism, and cosmology (Park et al. 2005; Choi et al. 2010; Way et al. 2011 among many others).

The genus as applied in cosmology quantifies the connectivity of iso-density or iso-temperature contour surfaces of smooth matter density or cosmic microwave temperature field, and is equal to  $-1/2$  times the Euler characteristic of the surface or equivalently a linear combination of the Betti numbers of the excursion sets, topological invariants of figures that can be used to distinguish topological spaces (see Park et al. 2013 for the relations among the genus, Euler characteristic, and the Betti numbers in two- and three-dimensions). The genus is also one of the parameters characterizing the geometry of figures called the Minkowski Functionals (Mecke et al. 1994; Pratten & Munshi 2012; Hikage et al. 2006; Hikage et al. 2008).

In the analysis of the topology of the observed LSS, as in many other cases, the genus directly measured from the observational data contains large systematic effects. It is thus critically important to accurately estimate the systematic effects and statistical uncertainties in order to draw any sensible conclusions. An example of extreme care of various systematic effects on the genus is the work by Choi et al. (2010) and Choi et al. (2013) where, in addition to sophisticated correction for the radial and angular selection effects in the observational data, a number of mock surveys performed within a large cosmological simulation mimicking the actual observation in detail are used to simulate the systematic effects produced by non-linear gravitational evolution, redshift-space distortion, shot noise in the smoothed density field, bias in the distribution of galaxies with respect to the underlying matter density field, and the finite size of the pixels used to build the density field. Without taking into account of these effects one would make completely wrong conclusions on the interpretation of the deviation of the measured genus curve from the Gaussian predictions. The primordial non-Gaussianity can be studied only through statistical comparison of observations with the accurately modeled mock survey samples in a simulated universe with well-defined initial conditions. Therefore, mock survey samples drawn from large-volume cosmological simulations are an essential element of topology analysis of LSS that enables

one to model all the systematics and to correctly estimate the statistical uncertainties in the derived cosmological parameters.

There have been a number of studies that tried to estimate some of these systematic effects individually. The finite pixel size effects have been analytically studied for the 3-dimensional genus by Hamilton et al. (1986) and the 2-dimensional genus by Melott et al. (1989). Melott et al. (1988) and Park & Gott (1991) numerically studied the combined effects of the non-linear gravitational evolution and galaxy biasing. An analytic formula for the effects of non-linear gravitational evolution has been found by Matsubara (1994, 2003) using the second-order perturbation theory, which was confirmed by Matsubara & Suto (1996) in the weakly nonlinear regime. The redshift-space distortion effects in the linear regime were found by Matsubara (1996). James (2012) discussed the systematic effects inducing non-Gaussianity in the genus statistic produced by galaxy bias, nonlinear gravitational evolution and primordial non-Gaussianity and presented a technique to decomposing them into an orthogonal polynomial sequence. The effect of non-periodic sample boundaries in conjunction with smoothing method, which is not dealt with in this paper, was studied by Melott & Dominik (1993).

In practice, the systematic effects in the genus measured from observations or mock surveys are all combined and reveal themselves as a composite deviation from the Gaussian curve. However, it is theoretically interesting to know the sign and magnitude of individual effects. With such understanding one can make a better control of individual effects and it would be possible to reduce them. In this paper we will measure the individual effects of these systematics using the matter density field and dark matter halo distribution obtained from a cosmological  $N$ -body simulation, the Horizon Run 2 (HR2), one of the largest cosmological simulations in terms of the number of particles evolved and the physical volume simulated (Kim et al. 2011).

The non-Gaussian deviations of the genus curve we will present are correct only for the particular cosmological model we adopt (a flat  $\Lambda$ CDM cosmology with the 5 year WMAP cosmological parameters) and the galaxy-subhalo correspondence model of galaxy assignment we adopt in this paper. However, it is believed that these models are reasonable approximations (for massive objects in particular) and any small changes in cosmology and galaxy assignment scheme would not change our conclusions on the nature of the non-Gaussian genus deviations due to systematic effects.

The paper is structured as follows. In Section 2 we briefly introduce the genus statistic. In Section 3 we explain the numerical simulation used in our study. Section 4 discusses the systematic effects and our modeling, and the summary and conclusion are given in Section 5.

## 2. The Genus Statistic

The genus is a measure of the topology of iso-density contour surfaces in a smoothed galaxy density field. In cosmology the genus is usually defined as (Gott et al. 1986)

$$G = \text{number of holes} - \text{number of isolated regions}, \quad (1)$$

where the “number of isolated regions” is the number of disconnected pieces into which the boundary surface is divided and the “number of holes” is the maximum number of cuts that can be made to the regions without creating a new disconnected region.

In the case of Gaussian fields, the genus per unit volume in the iso-density contour surface at a given threshold level  $\nu$ ,  $g(\nu) = G(\nu)/V$ , is known as (*e.g.* Doroshkevich 1970; Adler 1981; Hamilton et al. 1986)

$$g(\nu) = A(1 - \nu^2)e^{-\nu^2/2}. \quad (2)$$

The amplitude  $A$  is given by

$$A = -\frac{1}{8\pi^2} (\langle k^2 \rangle / 3)^{3/2}, \quad (3)$$

where  $\langle k^2 \rangle = \sigma_1^2 / \sigma_0^2$ . The spectral moments of the fields,  $\sigma_0$  and  $\sigma_1$  are computed from  $\sigma_0 = \sqrt{\langle \delta^2 \rangle}$ , and  $\sigma_1 = \sqrt{\langle |\nabla \delta|^2 \rangle}$ .  $\delta = (\rho - \bar{\rho}) / \bar{\rho}$  is the over-density field.

To separate the contribution of the one-point density distribution to the genus the volume-fraction threshold level has often been used in topology analyses (Weinberg et al. 1987). This parameter defines the iso-density contour surfaces in such a way that the volume fraction  $f$  in the high density region is equal to that of a Gaussian random field at the same threshold level, where

$$f = \frac{1}{\sqrt{2\pi}} \int_{\nu}^{\infty} e^{-x^2/2} dx. \quad (4)$$

This transformation of the density field, called Gaussianization, in general reduces the non-Gaussian features in the genus curve, but is useful when the non-Gaussianity of the primordial density field is to be studied (see Neyrinck et al. 2011 for matter density field, and Jee et al. 2012 for halo density field). We will use this parametrization in this paper for easier comparison with previous works, and the parameter  $\nu$  means the volume-fraction threshold.

## 3. Simulation

We use matter particle and dark halo data of an  $N$ -body simulation called Horizon Run 2 (HR2) that gravitationally evolved  $6000^3$  particles in a cubic comoving volume of

$(7200 h^{-1}\text{Mpc})^3$  (Kim et al. 2011). The simulation is based on the standard concordance model with parameters corresponding to the WMAP 5-year cosmology (Komatsu et al. 2009) of  $\Omega_\Lambda = 0.74$ ,  $\Omega_m = 0.26$ ,  $\Omega_b = 0.044$ ,  $n_s = 0.96$ ,  $h = 0.72$ , and  $\sigma_8 = 0.794$ . The particle mass is about  $1.25 \times 10^{11} h^{-1}\text{Mpc}$  and the mean particle separation is  $1.2 h^{-1}\text{Mpc}$ . The initial redshift of the simulation is  $z_i = 32$ . The initial particle distribution are generated by using the Zel’dovich approximation which adopts the first-order Lagrangian perturbation theory. Even though the small-scale ( $k \geq 0.2 h^{-1}\text{Mpc}$ ) power shows a subtle underestimation compared with the second-order scheme (L’Huillier et al. 2014), at low redshifts the Zel’dovich approximation does not show any noticeable difference for the smoothing scales that we are interested in here (Gaussian smoothing lengths from  $R_G = 15$  to  $34 h^{-1}\text{Mpc}$ )

We use the snapshot data of HR2 at  $z = 0$  in our study. The physical size of HR2 is large enough to correctly model the growth of LSS through coupling of density fluctuations on various scales and to allow us to measure all the systematics to great accuracies with negligible statistical uncertainties. To study the galaxy biasing effects on the genus, we adopt the subhalo-galaxy correspondence model (Kim et al. 2008) and assign a galaxy at the location of each dark halo. The dark matter halos are the physically self-bound (PSB) halos identified in HR2 using the method described in Kim & Park (2006). They are gravitationally self-bound, and tidally stable halos hosting a density maximum. Since a roughly volume-limited subsample of galaxies that can be extracted from the on-going SDSS-III BOSS survey for topology analyses has the mean galaxy separation of about  $15 h^{-1}\text{Mpc}$  (Choi et al. in preparation), we set the minimum halo mass of  $1.61 \times 10^{13} h^{-1}\text{M}_\odot$  (129 particles) so that the average PSB halo separation in HR2 becomes also  $15 h^{-1}\text{Mpc}$ . This subhalo-galaxy correspondence model has been proven to work well in terms of one-point function and its local density dependence (Kim et al. 2008), two-point function (Kim et al. 2009), and also topology in particular (Gott et al. 2009; Choi et al. 2010).

## 4. Systematic Effects and Modeling

### 4.1. Finite pixel size

The density field estimated from a discrete particle distribution and mapped onto a grid is affected by the finite pixel size and the way that the particle mass is divided into adjacent pixels. To study the effects as a function of pixel size we use a set of grids with cubic pixels and with size of 600, 720, 840, 900, 960, 1080, 1200, 1260, 1440, 1800, 1920, and 2160 in terms of number of pixels along a side. Since the physical size of HR2 is  $7200 h^{-1}\text{Mpc}$ , they correspond to 12, 10, 8.57, 8, 7.5, 6.67, 6, 5.71, 5, 4, 3.75, and 3.33  $h^{-1}\text{Mpc}$  respectively, in terms of pixel size  $p$ . We used the Cloud-in-Cloud (CIC; Hockney & Eastwood 1981) mass

assignment scheme in this study. The pixel densities are then smoothed over three different smoothing lengths,  $R_G = 15, 22,$  and  $34\text{Mpc}$ . These smoothing scales are motivated by the mean separations of galaxies in the SDSS-III BOSS CMASS sample ( $\bar{d} = 15 h^{-1}\text{Mpc}$ ) and SDSS-II LRG sample (Gott et al. 2009). The genus curves are obtained for each case of selected grid size and smoothing scale. Also we calculate the mean-square matter density  $\sigma_0$  and the mean square density gradient fluctuations  $\sigma_1$ .

Figures 1 and 2 show how the amplitude of the genus curves depends on the pixel size relative to the smoothing length. In Figure 2 the amplitude  $A$  is calculated for each  $p/R_G$  using the formula for Gaussian fields (Gott et al. 1986; Tomita 1986)

$$A = \frac{1}{(2\pi)^2} \left[ \frac{\sigma_1}{\sqrt{3}\sigma_0} \right]^3, \quad (5)$$

where  $\sigma_0$  and  $\sigma_1$  are directly calculated from the simulation. In many previous analyses of observational and simulation data a rule of thumb for choosing the pixel size was  $p = \sqrt{2}R_G/2.5$  or  $p/R_G = 0.566$  (Gott et al. 1989). As can be seen in Figure 2, such a choice results in underestimation of the genus amplitude by more than 5%.

In this section we aim to calculate the genus curves  $G(\nu; p/R_G)$  and  $G(\nu; p/R_G = 0)$  with and without the finite pixel size effects, respectively. Their difference is the systematic effects, which we model by the formula

$$\Delta G_{\text{pixel}}(\nu) = Ae^{-\nu^2/2} \times [aH_0(\nu) + bH_1(\nu) + cH_2(\nu) + dH_4(\nu)]p^2/R_G^2, \quad (6)$$

where  $H_i$ 's are the Hermite polynomials<sup>1</sup> and  $A$  is the amplitude of the genus curve of a Gaussian field having the same  $\sigma_0$  and  $\sigma_1$  measured with vanishing size pixels.

We find that this functional form very accurately model the pixel effects. This form is partly motivated by Hamilton et al. (1986), who predicted the odd function term  $bH_1$  to be absent.

Since we do not know the genus amplitude with no pixel effects in the beginning, we cannot calculate the difference  $\Delta G$  directly. We therefore obtain the genus amplitude and the coefficients at the same time iteratively. At the first step we calculate  $\Delta G$  and the coefficients assuming that the genus amplitude calculated according to Equation (5) from the density field constructed with the highest resolution approximates the genus with no

---

<sup>1</sup>  $H_i$ 's are the Hermite polynomials, and  $H_0(\nu) = 1$ ,  $H_1(\nu) = \nu$ ,  $H_2(\nu) = \nu^2 - 1$ ,  $H_3(\nu) = \nu^3 - 3\nu$ , and  $H_4(\nu) = \nu^4 - 6\nu^2 + 3$ .

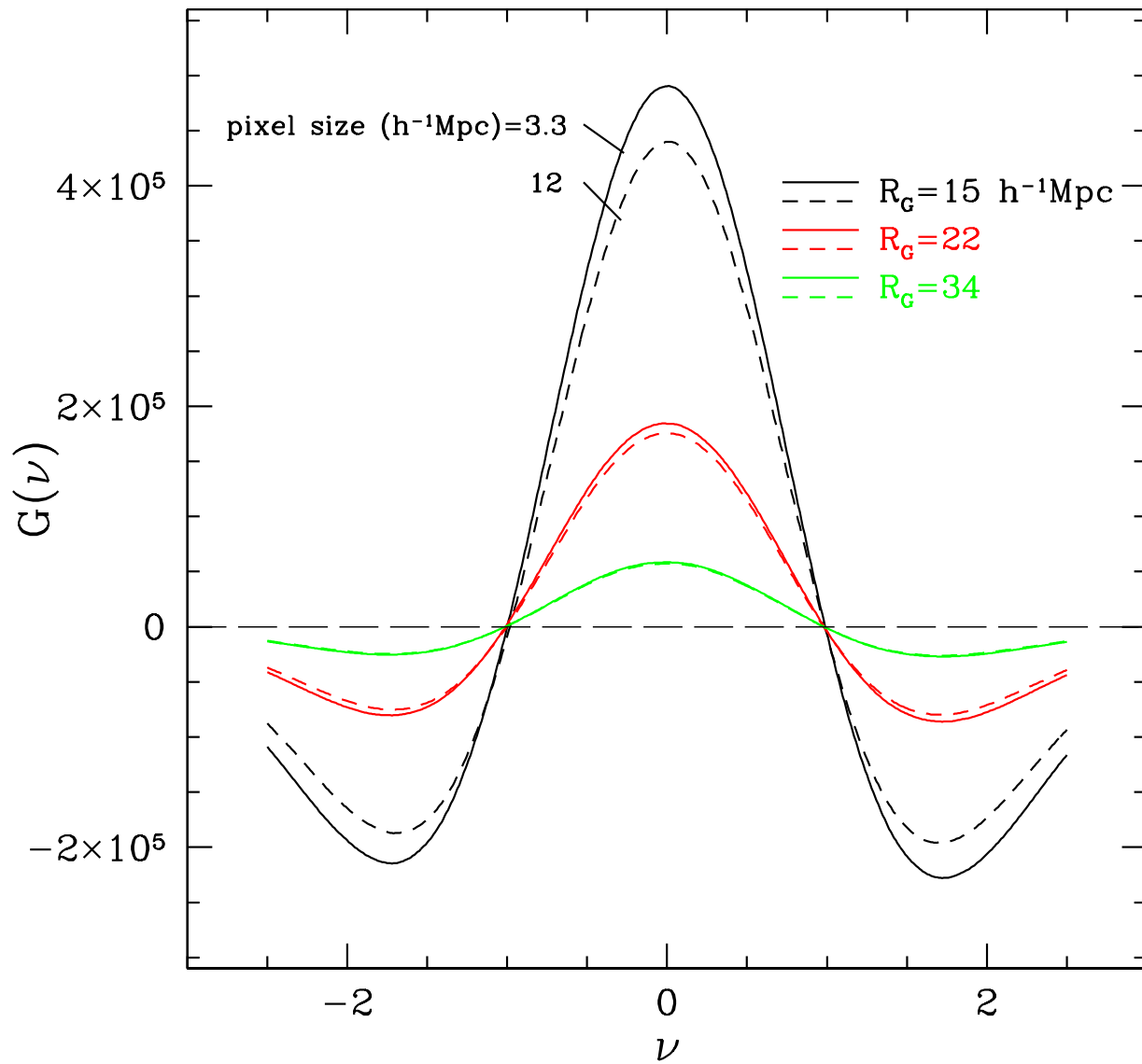


Fig. 1.— Pixel-size dependence of the genus curve on three smoothing scales. The solid (dashed) lines are the genus curve obtained with the grids of size  $p = 3.3(12) h^{-1}\text{Mpc}$ .

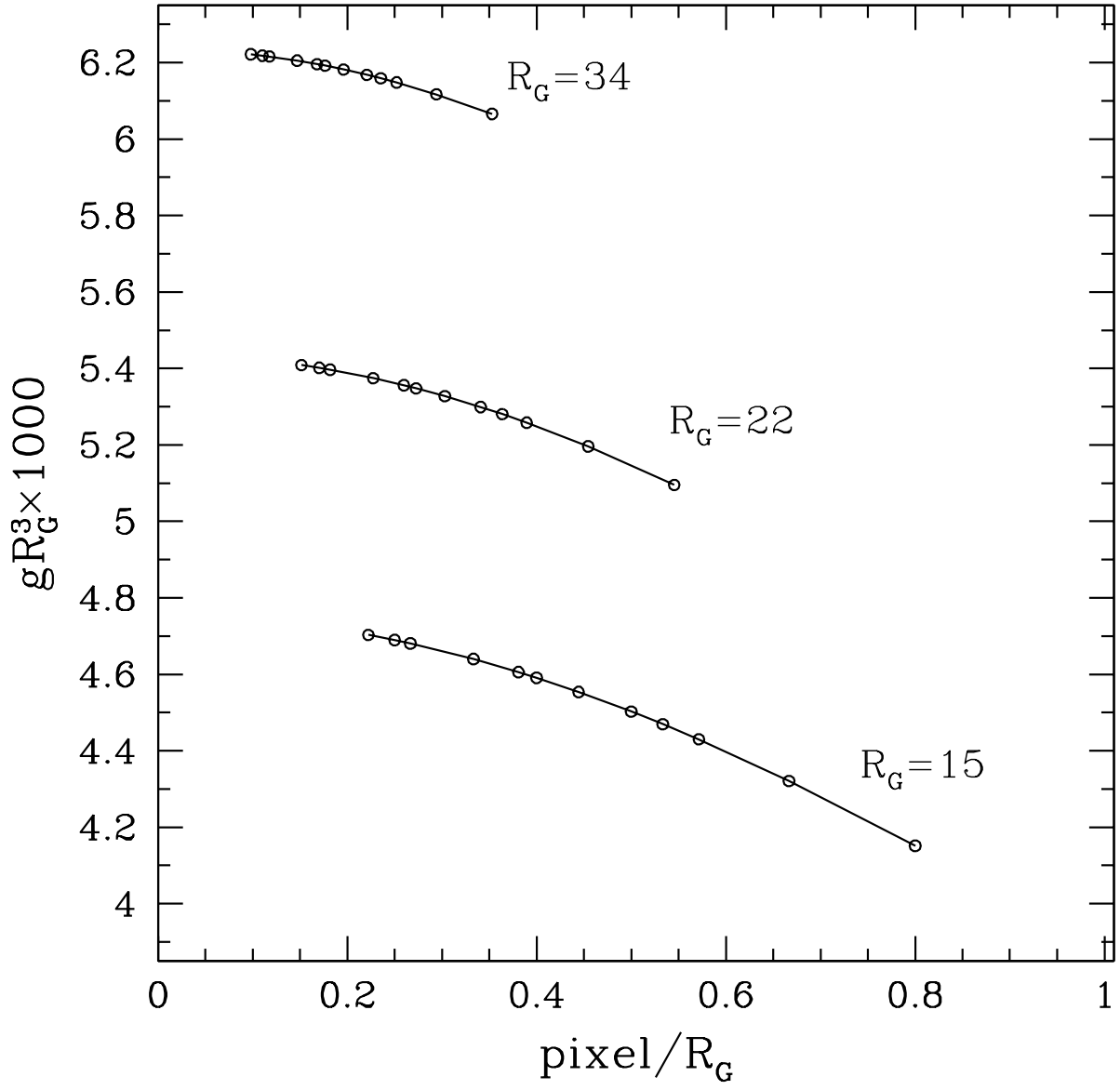


Fig. 2.— Dependence of the amplitude of the genus curve on the relative pixel size. The amplitude is calculated from Equation (5).



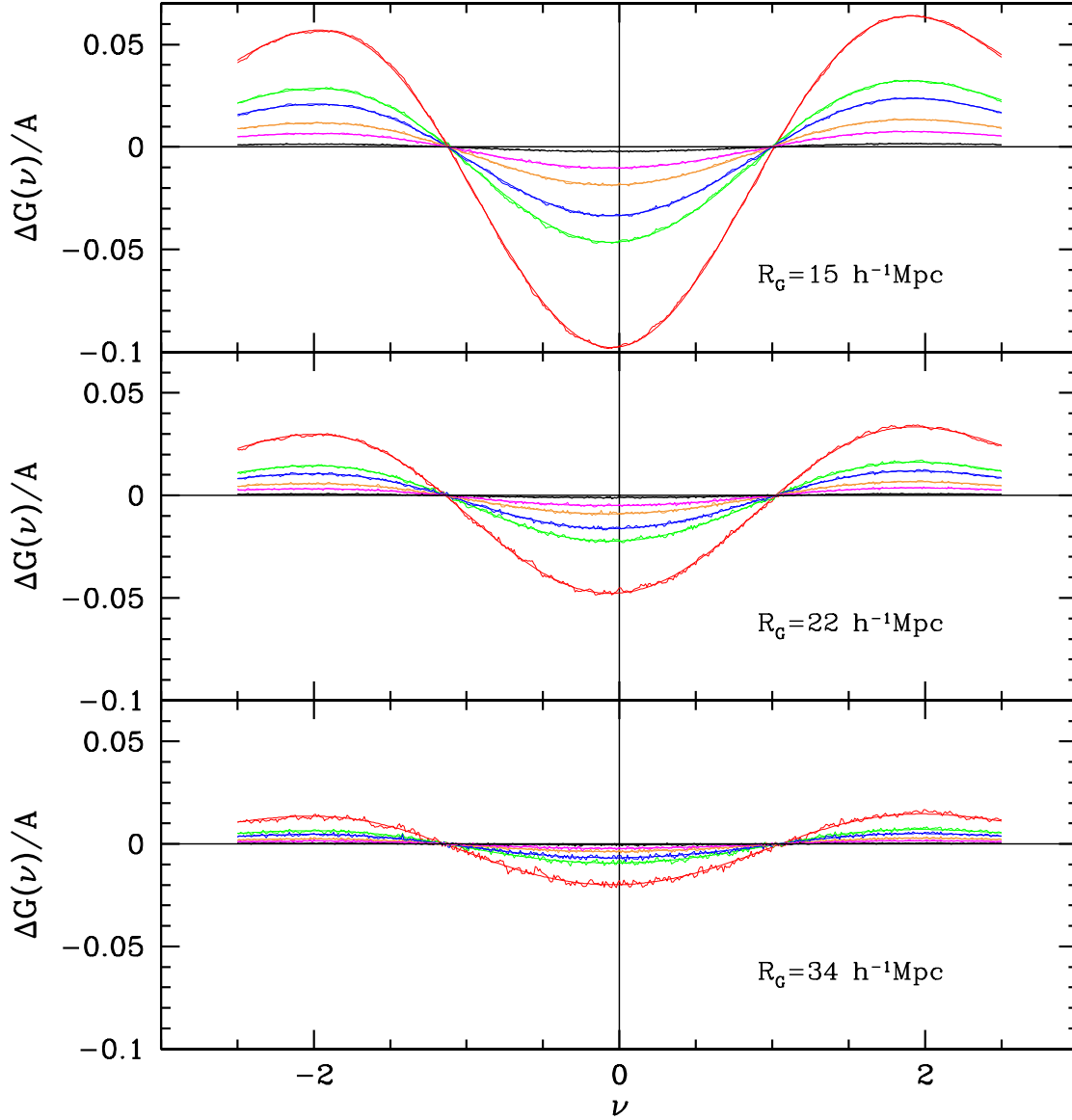


Fig. 3.— Deviations of the genus curve from the Gaussian value due to the finite pixel size effects. Each color denotes the pixel size - 3.33 (black), 5(magenta), 6(yellow), 7.5(blue), 8.57(green) and 12(red)  $h^{-1}$ Mpc.

pixel effects. In the next step the new amplitude is estimated using Equations (5) and (6) from  $A(p/R_G = 0) = A(p_s/R_G) - \Delta G(\nu = 0; p_s/R_G)$ , where  $p_s$  is the smallest pixel size. The updated amplitude  $A$  is 524268, 190332, and 59180 for  $R_G = 15, 22,$  and  $34 h^{-1}\text{Mpc}$ , respectively. From the updated amplitude the new  $\Delta G$  and coefficients are obtained.

To find the coefficients  $a, b, c,$  and  $d$  we carried out a chi-square ( $\chi^2$ ) minimization with Markov Chain Monte Carlo (MCMC) method by following the steps described in Verde et al. (2003) over ranges  $-2.5 < \nu < 2.5$ . We measure the coefficients for a set of values of  $p/R_G$ . For example, in the case of  $R_G = 15 h^{-1}\text{Mpc}$  we measure them for  $p/R_G = 0.222, 0.25, 0.267, 0.333, 0.381, 0.4, 0.445, 0.5, 0.533, 0.571, 0.667,$  and  $0.8$ . The smallest value corresponds to the biggest mesh  $2160^3$ , and the largest one to the smallest mesh  $600^3$ . The iterative process makes the coefficients independent of the pixel size as assumed in Equation (6). The set of coefficient values that minimize  $\chi^2$  are listed in Table 4.1 for three smoothing lengths. In Table 4 in Appendix A, we list the complete genus values relative to these measurements as a function of the volume fraction threshold  $\nu$ .

In Figure 3 we show the finite pixel size effects normalized by the genus amplitude without pixel effect. Shown are cases for  $p = 3.33, 5, 6, 7.5, 8.75,$  and  $12 h^{-1}\text{Mpc}$ . The smooth curves in the same color are the fits given by Equation (6) with the coefficients listed in Table 4.1. The fits are so excellent that it is difficult to distinguish between the numerical data and the corresponding fit. We dropped the term  $H_3$  in the final form of the model because we found its contribution is negligible.”

It can be seen in Figure 3 that if one follows Park et al. (2005), who argued that the pixel size should be smaller than the smoothing length at least by a factor three, the underestimation of the genus amplitude becomes less than 1%.

Hamilton et al. (1986) derived a formula for the pixel effects that includes the even Hermite polynomials such as  $H_0, H_2$  and  $H_4$ . But we find that the genus deviations are not exactly symmetric with respect to  $\nu = 0$  and an odd term ( $H_1$ ) is needed to better describe the pixel effects. This is because the high-density regions are more affected by the pixel smoothing. But it is still true that the even terms are dominant and the consequence brought by pixel effects on the genus curve is mostly the amplitude drop.

## 4.2. Non-linear gravitational evolution

The genus of the large-scale density field is insensitive to the non-linear gravitational evolution because it remains the same as far as the connectivity of structures does not change, regardless of change in the amplitude or shape of the fluctuations. This makes the genus

a better tool for a cosmological probe than galaxy power spectrum or correlation function where it is not so easy to model and remove the large non-linear effects (see Figs. 4-6 and 11 of Kim et al. 2009). The deviation of the genus curve from its Gaussian form has been studied in many literatures (Melott et al. 1988; Park & Gott 1991; Weinberg & Cole 1992; Matsubara 1994, 2003; Park et al. 2005; Hikage et al. 2003, 2006), where most of the analytic derivations are based on the second-order perturbation theory.

To estimate the non-linear gravitational evolution effects on the genus deviations, we measure the genus curves of the initial matter density field (at  $z = 32$ ) and of the final matter density field (at  $z = 0$ ) using a large array of  $2160^3$  pixels to minimize the pixel effects. In Table 5 in Appendix A, the genus values are given as a function of the volume fraction threshold,  $\nu$ .

Figure 4 shows the genus curves of the initial and final matter density fields, which clearly show amplitude drop due to the nonlinear gravitational evolution. The gravitational evolution affects the topology of low-density regions more seriously. This is because, as the gravitational evolution progresses, expanding low-density regions percolate with one another by opening their outer boundaries, and the number of disconnected voids decreases. On the other hand, the high-density regions contract to remain as density peaks surrounded by less dense regions unless they happen to have very close merging pairs.

We compute the difference of the genus ( $\Delta G_{\text{grav}}$ ) between the initial matter density field at  $z_i = 32$  and the final matter density field at  $z_f = 0$  as

$$\Delta G_{\text{grav}}(\nu, z, R_G) = G(\nu, z_f, R_G) - G(\nu, z_i, R_G), \quad (7)$$

and normalize it with the genus amplitude using Equation (5). Since all other conditions are fixed, this will give us the sole effect of non-linear gravitational evolution.

Matsubara (1994, 2003) derived an explicit formula for the genus due to the gravitational evolution including nonlinear terms from the second order perturbation theory. For three-dimensional genus and when the volume-fraction thresholds are used, this has the form of

$$G(\nu) = -Ae^{-\nu^2/2} \times [H_2(\nu) + [(S^{(1)} - S^{(0)})H_3(\nu) + (S^{(2)} - S^{(0)})H_1(\nu)]\sigma_0] \quad (8)$$

where  $S^{(i)}$  are the skewness parameters (see Matsubara 2003 for their definitions).

Figure 5 shows the difference calculated from the simulation results (top panel) and that from the analytic prediction by Matsubara (bottom panel). In Table 2, we summarize the values of  $A$ ,  $\sigma_0$ ,  $\sigma_1$ , and fitting coefficients. According to the Matsubara's formula, the genus

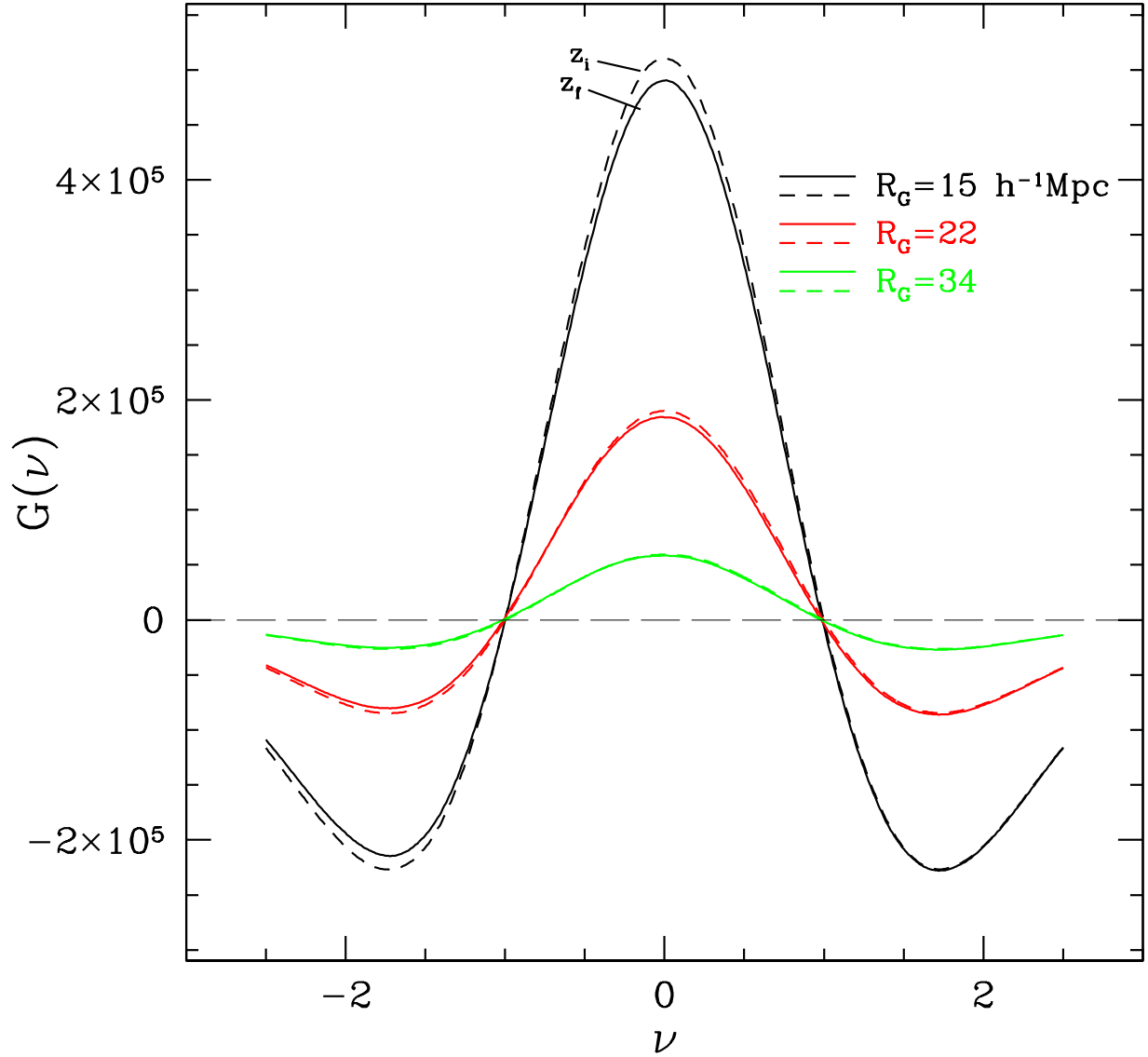


Fig. 4.— Gravitational evolution effects on the genus curve. The solid and dashed curves are the genus measured from the density fields at the initial ( $z_i = 32$ ) and final ( $z_f = 0$ ) epochs, respectively.

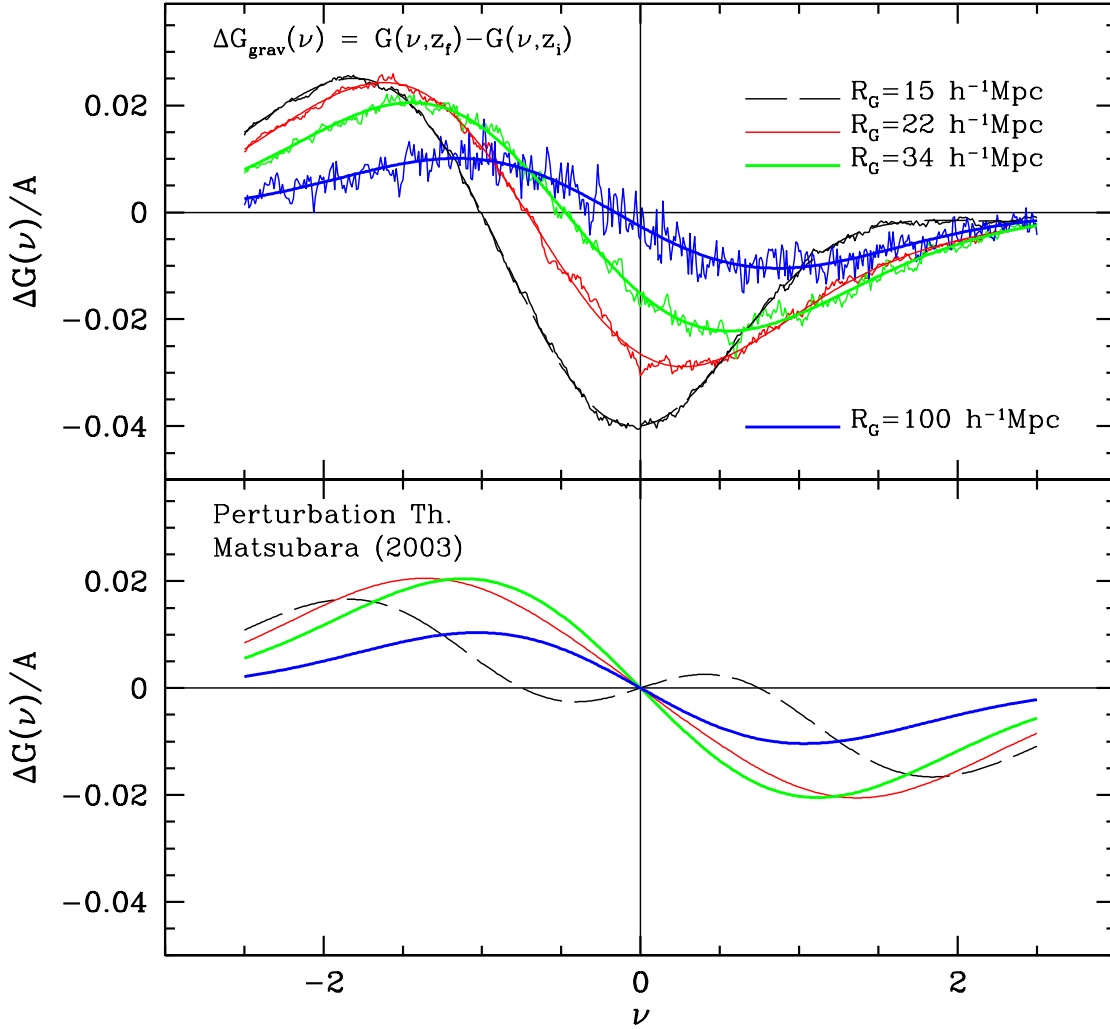


Fig. 5.— Deviations of the genus curve from the Gaussian function due to the gravitational evolution at four smoothing scales. Curves in the upper panel are from simulation, and those in the lower panel are predictions by the perturbation theory. In the top panel, the curves with jitters are the numerically measured genus deviations and the smooth curves are fitting functions using the Hermite polynomials up to the 4th order. At  $R_G = 100 h^{-1}\text{Mpc}$ , the perturbation theory well agrees with the simulation.

deviations should be symmetric with respect to the origin with opposite sign, and at  $\nu = 0$  the genus deviation is expected to be null. On the other hand, the simulation measurement shows that the deviation is far from symmetric and there is a significant drop at  $\nu = 0$ .

We note that the measured  $\Delta G_{\text{grav}}$  is significantly shifted towards the low density regions. The amplitude drop implies that there need terms with even orders ( $H_{2n-2}$ ). We model  $\Delta G_{\text{grav}}$  as follows:

$$\Delta G_{\text{grav}}(\nu) = Ae^{-\nu^2/2} \times [(bH_1(\nu) + dH_3(\nu))\sigma_0 + (aH_0(\nu) + cH_2(\nu))\sigma_0^2]. \quad (9)$$

$A$  is again the genus amplitude estimated from the Gaussian formula (Eq. 5), where  $\sigma_0$  and  $\sigma_1$  are directly measured from the initial density field and linearly extrapolated to  $z = 0$  (rather than the final density field). In this equation, the first two terms in the square bracket can be also found in Equation (8) and the other terms with even functions are added to model the rest of deviations due to high-order non-linearities. In Table 2 we show that as the smoothing length increases, the coefficients of the Hermite polynomials calculated from the perturbation theory,  $S^0 - S^1$  and  $S^0 - S^2$  become in good agreement with the coefficients  $b$  and  $d$  in Equation (9), respectively. In other words, the significant discrepancy between the gravitational effects found in simulation and the Matsubara’s prediction is mainly due to the lack of the even functions in the analytic formula. The *r.m.s.* density fluctuation on  $R_G = 15, 22$ , and  $34h^{-1}\text{Mpc}$  scales is 0.2604, 0.1763, and 0.1080, respectively (see Tab. 2). The agreement becomes much better for  $R_G = 100h^{-1}\text{Mpc}$  when  $\sigma_0 = 0.0243$  (see the blue curves in Fig. 5).

We overplot the best fit model (smooth curves) in the top panel of Figure 5 to demonstrate that our model describes the gravitational evolution much more accurately than Matsubara’s. Since our simulated genus is different from the analytical prediction, we take one more step to cross check the dependence of the genus on  $\sigma_0$  in Equation (9). We use the HR2 simulation cube data at four redshifts ( $z = 2, 1, 0.5$ , and 0) to measure  $\sigma_0$  and the genus, and fit the genus with Equation (9). The behavior of the coefficients of the Hermite polynomials is shown in Figure 6. During the measurement, we use the simplified coefficients such as  $\alpha \equiv Aa\sigma_0^2$  and  $\gamma \equiv Ac\sigma_0^2$ . The figure shows that the coefficients for  $H_0$  and  $H_2$  have quadratic dependence on  $\sigma_0$ , validating our fitting model. This means that we need not only a linear order term in  $\sigma_0$  but also the second-order terms. Therefore, adding one more term to the perturbation theory up to the second order in  $\sigma_0$  will produce a significantly better fit to the simulated data.

Table 1: Coefficients for pixel effects

$\Delta G_{\text{pixel}}/A = e^{-\nu^2/2}[aH_0 + bH_1(\nu) + cH_2(\nu) + dH_4(\nu)]p^2/R_G^2$												
$p$	$R_G = 15 h^{-1}\text{Mpc}$				$R_G = 22 h^{-1}\text{Mpc}$				$R_G = 34 h^{-1}\text{Mpc}$			
	$a$	$b$	$c$	$d$	$a$	$b$	$c$	$d$	$a$	$b$	$c$	$d$
3.33	0.0347	0.0197	0.2866	0.0294	0.0446	0.0228	0.3300	0.0377	0.0515	0.0175	0.3597	0.0454
3.75	0.0390	0.0214	0.2982	0.0313	0.0481	0.0235	0.3389	0.0395	0.0527	0.0194	0.3637	0.0464
4.00	0.0429	0.0230	0.3054	0.0325	0.0501	0.0232	0.3405	0.0397	0.0562	0.0185	0.3642	0.0457
5.00	0.0440	0.0234	0.3076	0.0329	0.0450	0.0248	0.3410	0.0350	0.0539	0.0192	0.3633	0.0462
5.71	0.0441	0.0234	0.3089	0.0334	0.0511	0.0246	0.3436	0.0404	0.0538	0.0201	0.3607	0.0451
6.00	0.0454	0.0244	0.3102	0.0335	0.0504	0.0234	0.3398	0.0397	0.0534	0.0190	0.3577	0.0444
6.67	0.0463	0.0239	0.3105	0.0334	0.0512	0.0268	0.3423	0.0401	0.0546	0.0200	0.3605	0.0462
7.50	0.0465	0.0231	0.3111	0.0335	0.0508	0.0244	0.3358	0.0382	0.0548	0.0166	0.3625	0.0461
8.00	0.0457	0.0238	0.3094	0.0336	0.0507	0.0246	0.3415	0.0403	0.0538	0.0201	0.3579	0.0441
8.57	0.0447	0.0240	0.3054	0.0328	0.0499	0.0248	0.3391	0.0397	0.0496	0.0229	0.3481	0.0427
10.00	0.0432	0.0228	0.3021	0.0325	0.0490	0.0235	0.3357	0.0394	0.0527	0.0181	0.3506	0.0444
average:	0.0433	0.0230	0.3050	0.0326	0.0496	0.0242	0.3389	0.0395	0.0534	0.0192	0.3590	0.0451

Note. — Pixel size  $p$  is in units of  $h^{-1}\text{Mpc}$ . Amplitude  $A$  is 524268, 190332, and 59180 for  $R_G = 15, 22,$  and  $34 h^{-1}\text{Mpc}$ , respectively.

Table 2: Coefficients for gravitational evolution effects for the matter density fields

$\Delta G_{\text{grav}}/A = e^{-\nu^2/2}[(bH_1 + dH_3)\sigma_0 + (aH_0 + cH_2)\sigma_0^2]$							
$R_G$	$a$	$b$	$c$	$d$	$\Delta_{r.m.s.}$	$\sigma_0$	$\sigma_1$
15	-0.1365	-0.1317	0.4523	-0.0487	3.9E-4	0.26039	0.01703
22	-0.1750	-0.2310	0.6779	-0.0433	6.9E-4	0.17634	0.00830
34	-0.2247	-0.3334	1.0791	-0.0336	7.4E-4	0.10797	0.00345
100	-0.6263	-0.7127	3.8696	-0.0151	8.1E-4	0.02429	0.00031
$\Delta G_{\text{grav}}^{\text{PT}}/A_{\text{LT}} = e^{-\nu^2/2}[(S^{(0)} - S^{(2)})H_1 + (S^{(0)} - S^{(1)})H_3]\sigma_0$							
$R_G$	$S^{(0)} - S^{(2)}$	$S^{(0)} - S^{(1)}$	$\sigma_0$	$\sigma_1$			
15	-0.1616	-0.0662	0.26225	0.01727			
22	-0.2732	-0.0501	0.17665	0.00837			
34	-0.3727	-0.0313	0.10759	0.00345			
100	-0.7494	-0.0212	0.02418	0.00031			

Note. — Smoothing length  $R_G$  is in units of  $h^{-1}\text{Mpc}$ . The smallest pixel size of  $p = 3.33 h^{-1}\text{Mpc}$  is used to minimize the pixel effect. Amplitude  $A$ , directly measured from the matter density field is 509401, 189590, 59366, and 3791 for  $R_G = 15, 22, 34,$  and  $100 h^{-1}\text{Mpc}$ , respectively.  $\Delta_{r.m.s.}$  is calculated from  $\sqrt{\sum_{j=1}^N \frac{1}{N} [\Delta G_{\text{grav}}^{\text{sim}}(\nu_j)/A - \Delta G_{\text{grav}}(\nu_j)/A]^2}$  where  $\Delta G_{\text{grav}}^{\text{sim}}(\nu_j)$  is from simulation (Eq. 7) and  $\Delta G_{\text{grav}}(\nu_j)$  is from the best-fit function (Eq. 9). Amplitude  $A_{\text{LT}}$  is the prediction from linear theory.

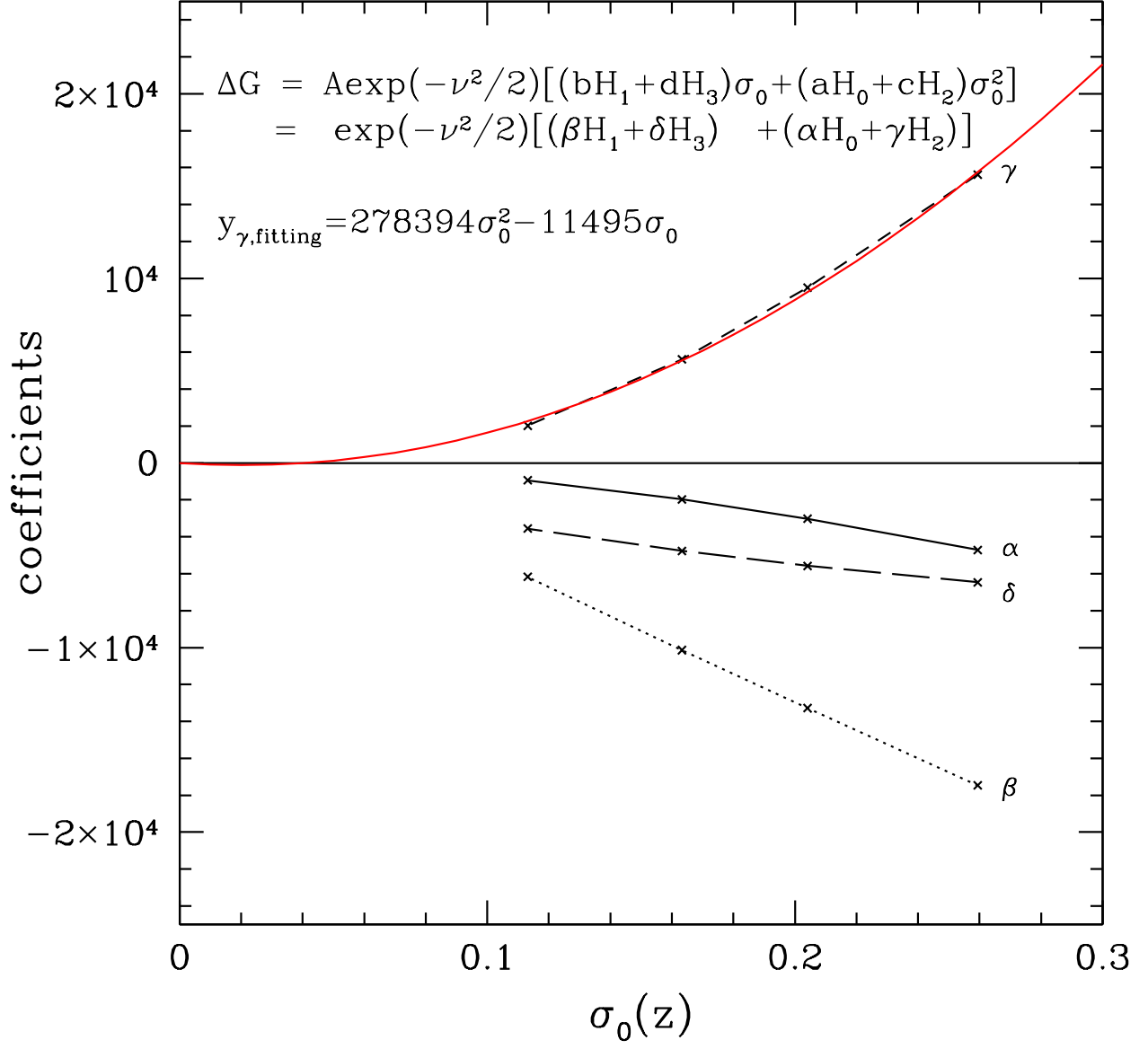


Fig. 6.— Change of the fitting coefficients with the standard deviation of the matter density field. Here, we use the definitions,  $\alpha \equiv Aa\sigma_0^2$ ,  $\beta \equiv Ab\sigma_0$ ,  $\gamma \equiv Ac\sigma_0^2$ ,  $\delta \equiv Ad\sigma_0$



### 4.3. Redshift-space distortion

In order to quantify the redshift-space distortion (RSD) effects on the genus curve, we compute the genus of the matter and halo density fields in real and redshift spaces. We again use the smallest possible pixel size ( $2160^3$  mesh for matter and  $2100^3$  mesh for halos) to minimize any unwanted other systematic effects. In Table 6 in Appendix A, the genus curves are given as a function of  $\nu$ .

Matsubara (1996) derived an analytical expression for the RSD effects on the genus curve in the linear regime as follows:

$$G_z(\nu) = \frac{3\sqrt{3}}{2}\sqrt{C}(1-C)G_r(\nu), \quad (10)$$

where  $G_z(\nu)$  and  $G_r(\nu)$  are the genus curves in redshift space and real space, respectively, and  $C \equiv C_1/C_0$ . According to Matsubara (1996),

$$C_j \equiv \frac{1}{2} \int_{-1}^1 d\mu \mu^{2j} (1 + fb^{-1}\mu^2)^2, \quad (11)$$

where  $b$  is the constant bias factor,  $f \equiv d \ln D / d \ln a$ ,  $D$  is the growth factor, and  $a$  is the cosmic expansion parameter. This formula suggests that the RSD does not change the shape of the genus curve but reduces its amplitude. This linear theory prediction does not agree well with our results on the smoothing scales we study as shown below.

In Figure 7 we plotted genus curves in real (solid) and redshift (dashed lines) spaces. In the top panel, we plotted genus curves for matter density field at  $z = 0$ . As one can see, the genus amplitude in the high density regions increases slightly more than in the low density regions. The halo density field shows a smaller amplitude drop than the matter density field, which implies that halos, being the massive objects, are less susceptible to RSD than matter.

With the definition of  $\Delta G_{\text{RSD}} \equiv G_z - G_r$ , we quantify the effects of RSD and fit the results with the fitting function

$$\begin{aligned} \Delta G_{\text{RSD}}(\nu) &= A e^{-\nu^2/2} \times \\ &[aH_0(\nu) + bH_1(\nu) + cH_2(\nu) + dH_3(\nu)], \end{aligned} \quad (12)$$

where the amplitude  $A$  is estimated using the Gaussian formula for the matter (or halo) density fields in real space. The change in the genus is well-modeled with a combination of Hermite polynomials up to the third order (see top panel of Fig. 8 for the matter density field and bottom panel for the halo density field). The values of coefficients are listed in Table 4.3.

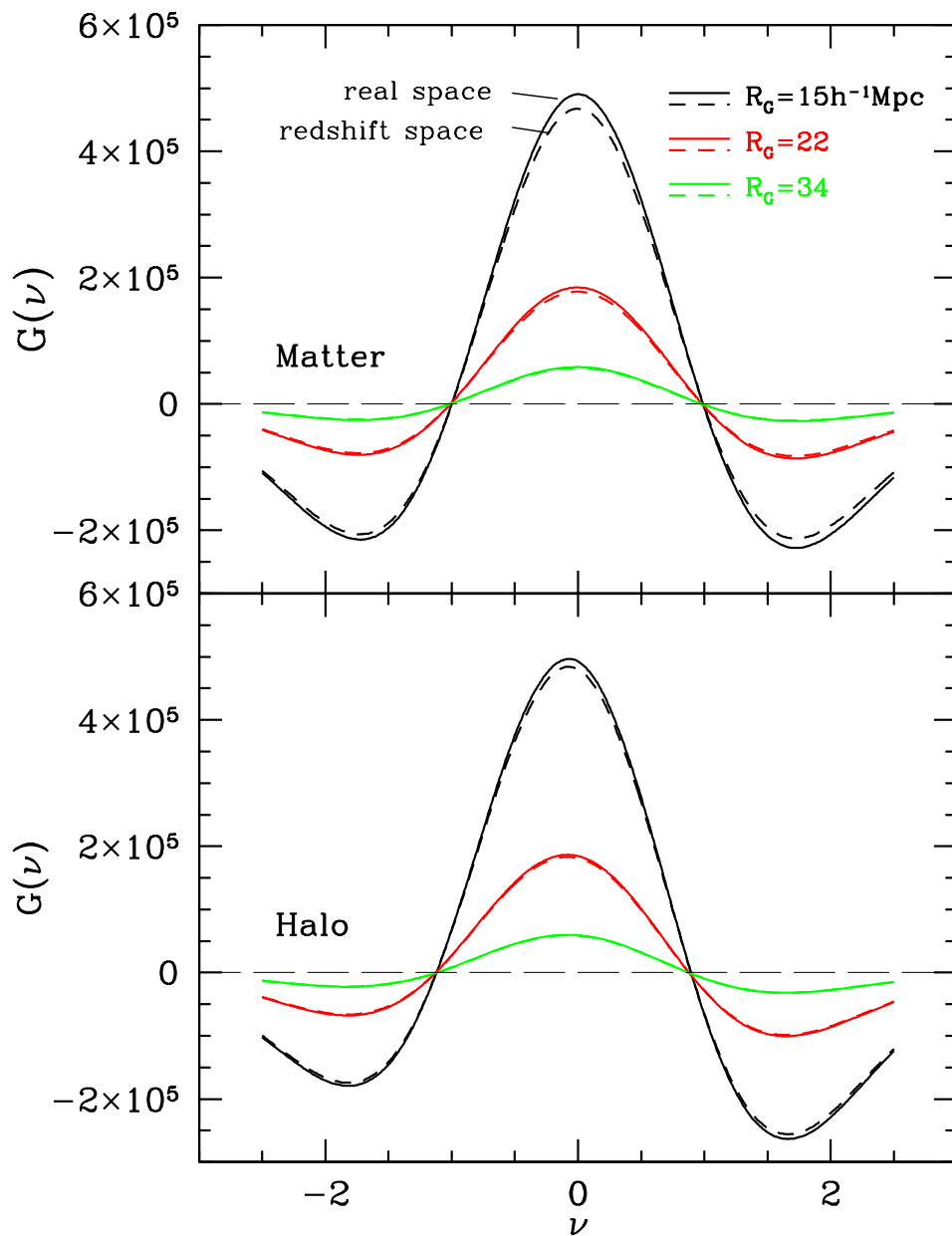


Fig. 7.— Genus curves in redshift (dashed) and real (solid lines) spaces for matter (top) and halo (bottom panel) density fields at three smoothing scales,  $R_G = 15$  (black), 22 (red), and 34  $h^{-1}\text{Mpc}$  (green). The redshift distortion reduces the genus amplitude in both matter and halo samples. Halo is less susceptible to redshift distortion.

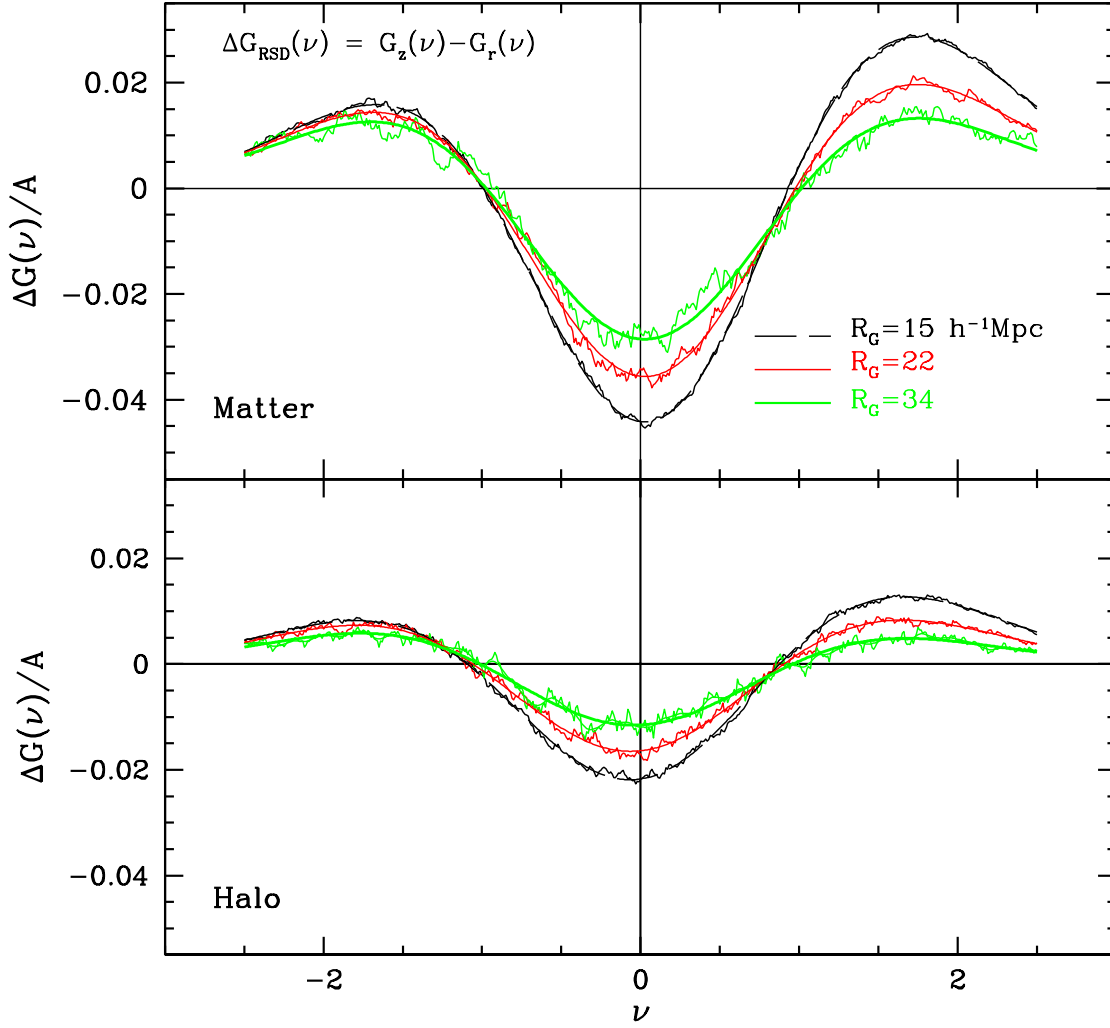


Fig. 8.— Effects of the redshift-space distortion on the genus in the matter density field (top) and in the halo density field (bottom). Y-axis is the normalized genus deviations caused by the redshift-space distortion. The jittering lines are obtained from simulation and smooth curves are our best fit models.

It can be seen in these figures that the genus in the high density regions decreases more compared to that in low density regions. This clearly indicates that the asymmetry is produced by the excessive mergers of high-density regions along the line of sight directions. The odd terms ( $H_1$  and  $H_3$ ) in the model explain the asymmetry. Although the coefficients  $b$  and  $d$  of the  $H_1$  and  $H_3$  for  $R_G = 15$  and  $22 h^{-1}\text{Mpc}$  listed in Table 4.3 are very small values, they are significantly non-zero. The asymmetry disappears rapidly as the smoothing length increases.

#### 4.4. Shot noise effects and halo biasing

Discrete sampling of an underlying density field at finite number of points produces the shot noise effects on the genus. The situation is more complicated when we study the halo (or galaxy) density field because the shot noise and the halo biasing effects are entangled. Separating these two effects is hard because the halos with mass above a given value is intrinsically sparse and we cannot avoid studying these effects in combination.

First, we study the pure shot noise effects in dark matter distribution. For each of three smoothing lengths, we have randomly sampled simulation particles at  $z = 0$  to have mean particle separations of  $\bar{d}/R_G = 0.08, 0.16, 0.32, 0.64, 1.0, \sqrt{2}, \sqrt{3}, 2.0, \text{ and } \sqrt{5}$ . In this case, we used the smallest pixel size (or the mesh size of  $2160^3$ ). In Table 7 in Appendix A, the genus values are given as a function of  $\nu$ . In the top panel of Figure 9, we plot genus curves for the smallest (solid lines) and the biggest  $d/R_G$  (dashed lines). As  $d/R_G$  increases, the genus curve shifts to the low density regions and the amplitude changes differently in low and high density regions. High density regions suffer from shot noise much more than low density regions. This is because some structures become split into multiple objects as we take out dark matter particles in the high density region, resulting in more isolated regions. The distortion of the genus curve is much larger compared to all the other systematic effects discussed so far.

We estimate the genus deviation due to the shot noise from  $\Delta G_{\text{shot}} \equiv G(\nu, \bar{d}/R_G) - G(\nu, \bar{d}/R_G = 0)$  with the approximation that  $G(\nu, \bar{d}/R_G = 0) \approx G(\nu, \bar{d}/R_G = 0.08)$ . Again, we model this difference using the Hermite polynomials as,

$$\Delta G_{\text{shot}}(\nu) = Ae^{-\nu^2/2} \times [aH_0(\nu) + bH_1(\nu) + cH_2(\nu) + dH_3(\nu) + eH_4(\nu)]. \quad (13)$$

Figure 10 shows that the model (smooth solid lines in red) describes the measured genus deviations (black lines) very well. The best-fit coefficients  $a, b$  and  $e$  are very small for small  $\bar{d}/R$  until  $\bar{d}/R \simeq 1.0$  (see Fig. 11). Coefficients  $c$  and  $d$  move in the opposite directions

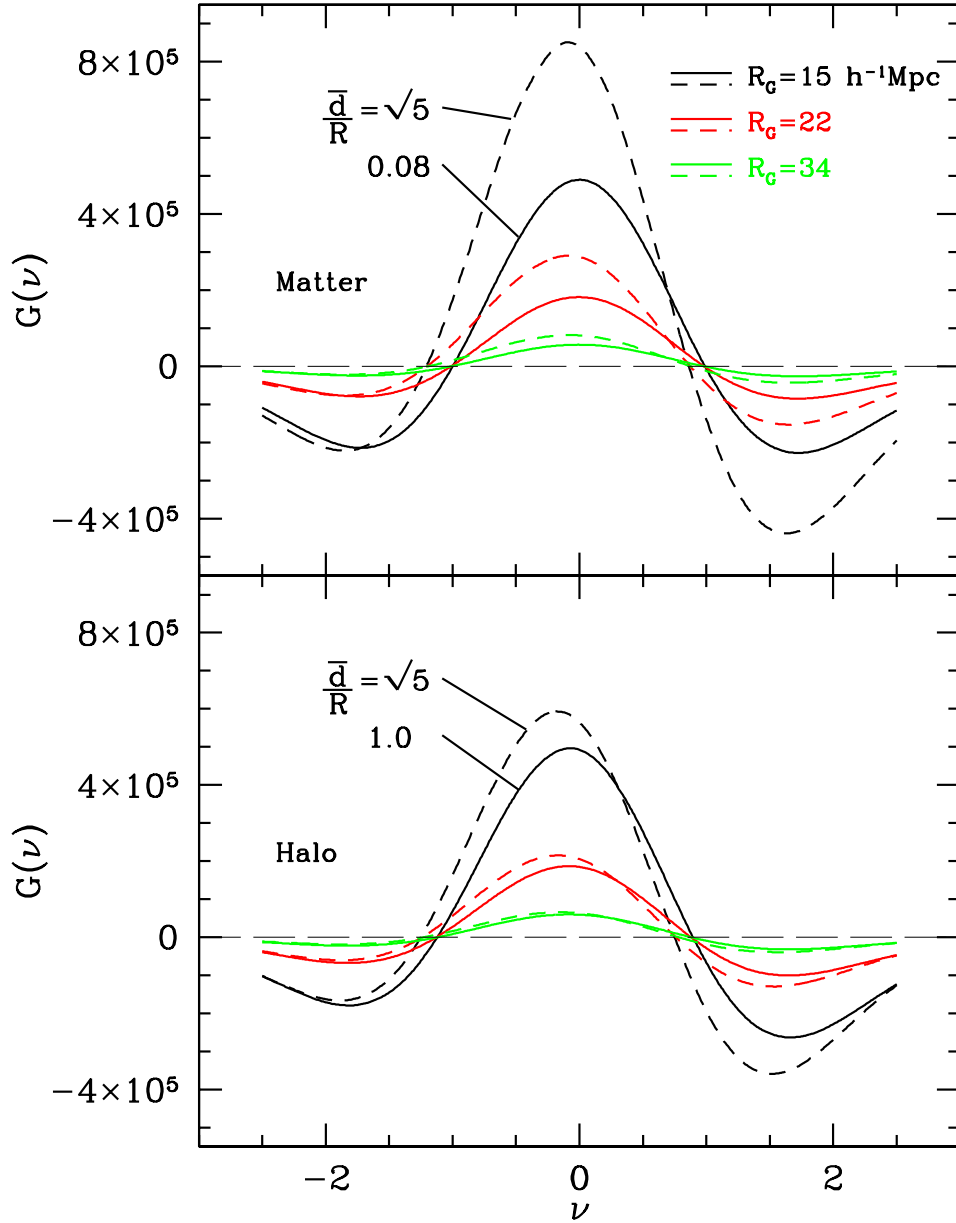


Fig. 9.— Effects of shot noise in the matter density field (top) and in the halo density field (bottom). Dashed lines are the genus for  $\bar{d}/R_G = \sqrt{5}$ , and solid lines are for  $\bar{d}/R_G = 0.08$  (matter) and 1 (halo). Black, red, and green curves are obtained using  $R_G = 15, 22,$  and  $34 h^{-1}\text{Mpc}$ , respectively. The shot noise not only changes the genus amplitude but also shifts the genus curve to the low density region, which breaks the symmetry of the genus curve.

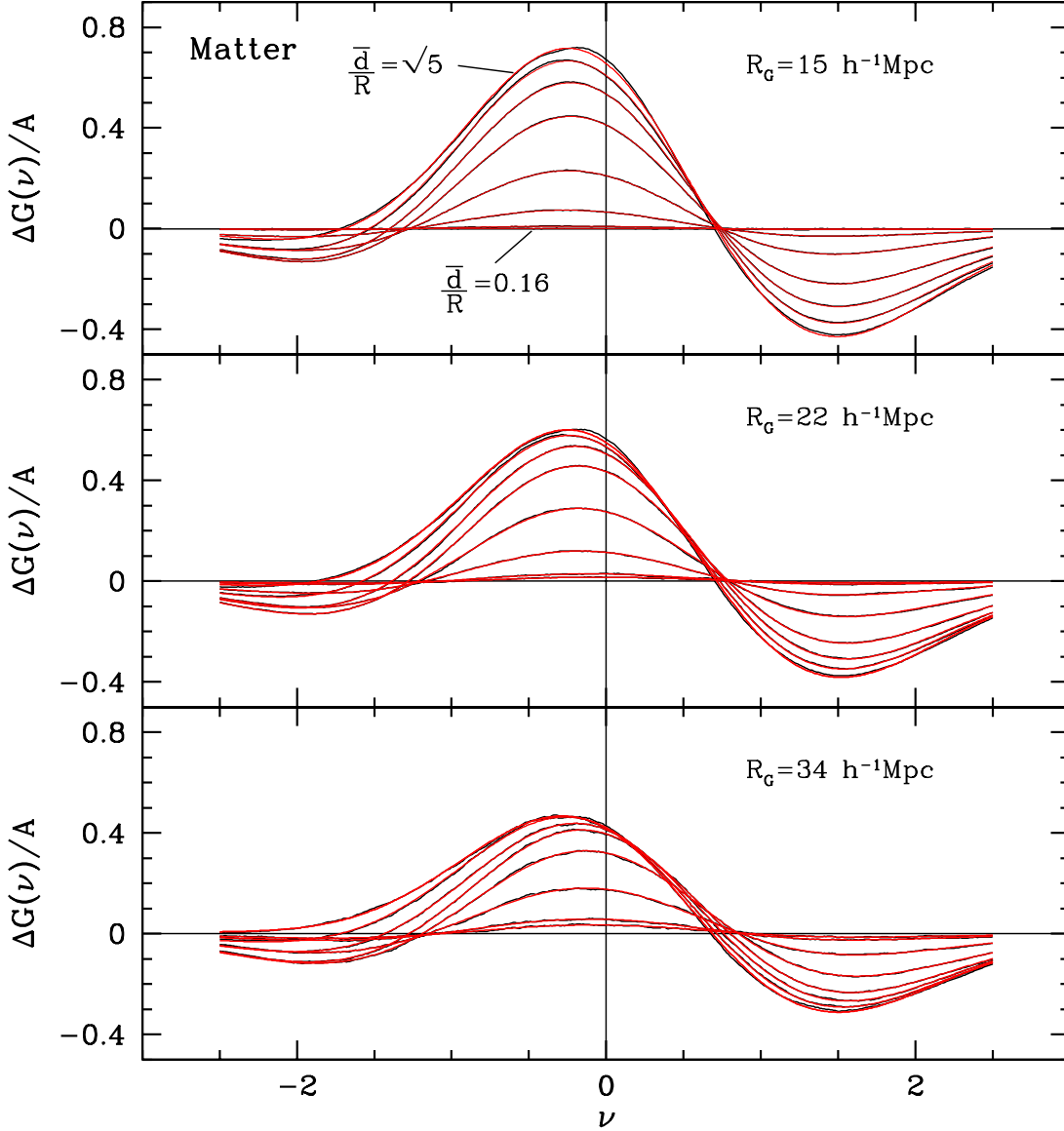


Fig. 10.— Genus deviation of the matter density fields for various mean separations ( $R_G = 15, 22, \text{ and } 34 \text{ h}^{-1} \text{ Mpc}$  from the top, middle, and bottom panels, respectively). From the top curve in each panel,  $\bar{d}/R_G = \sqrt{5}, 2, \sqrt{3}, \sqrt{2}, 1, 0.64, 0.32, \text{ and } 0.16$ . Also we show the fitting curves in the red color.

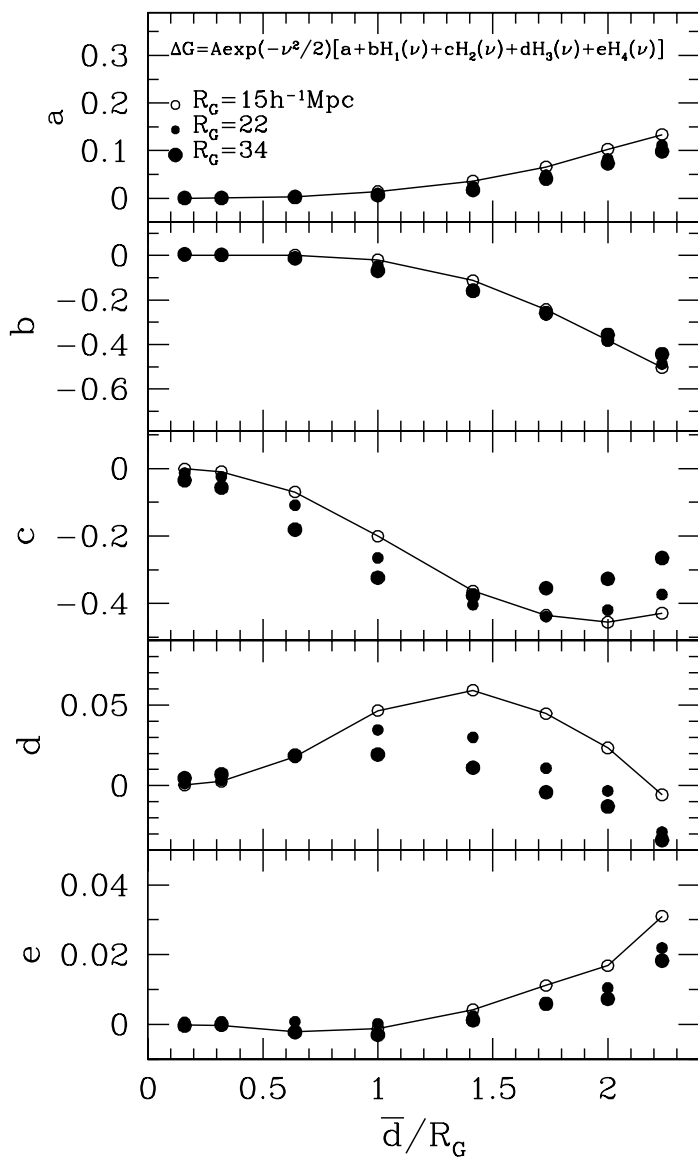


Fig. 11.— Fitting coefficients  $a, b, c, d$  and  $e$  for matter density fields. The open circles are for  $R_G = 15$ , small filled circles are for  $R_G = 22$ , and large filled circles are for  $R_G = 34 h^{-1} \text{Mpc}$ .

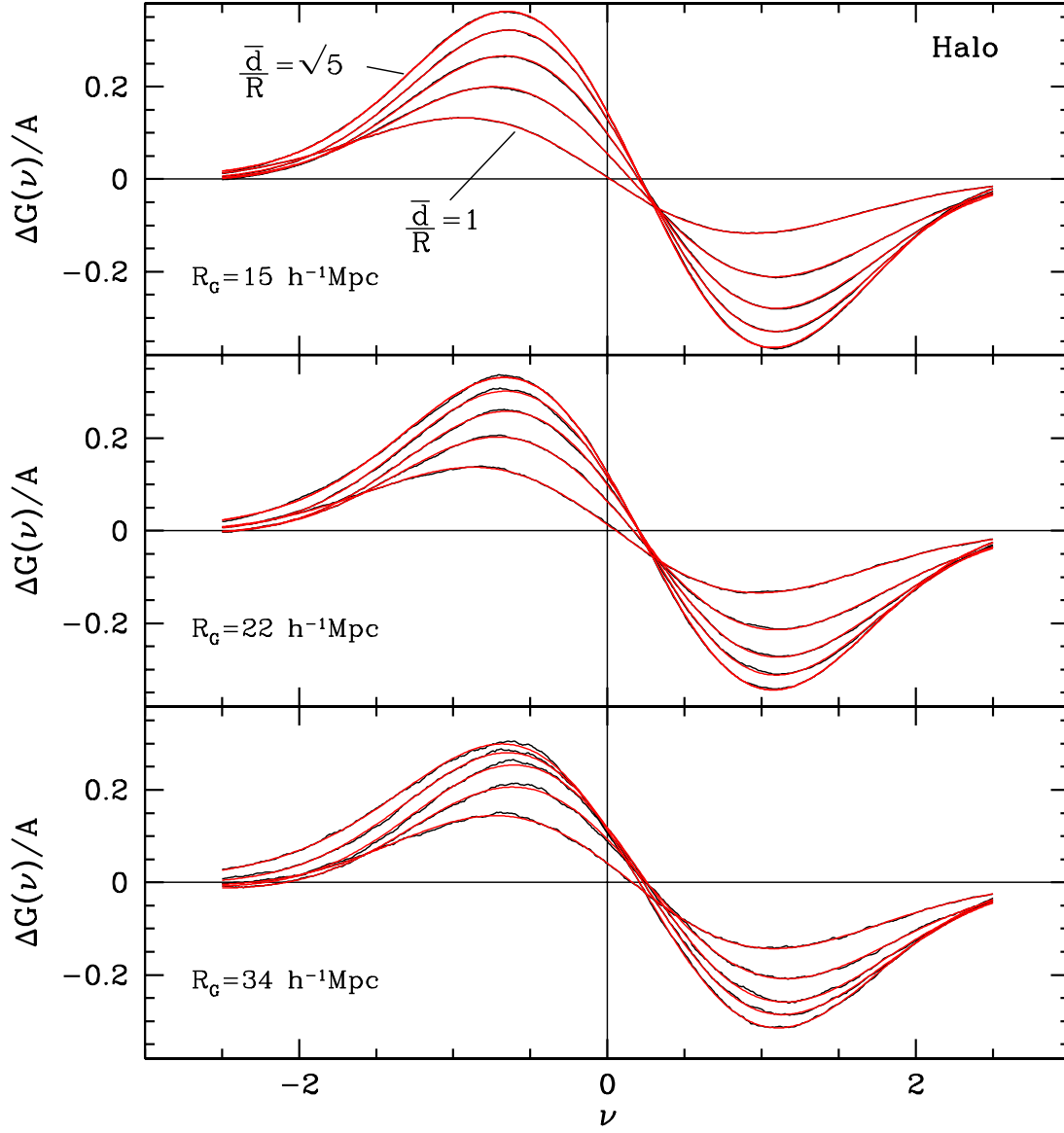


Fig. 12.— Same as Figure 10, but for halo density fields. Y axis is the deviation of halo genus from the matter genus of no shot noise. From the top curve,  $\bar{d}/R = \sqrt{5}, 2, \sqrt{3}, \sqrt{2}$  and 1.



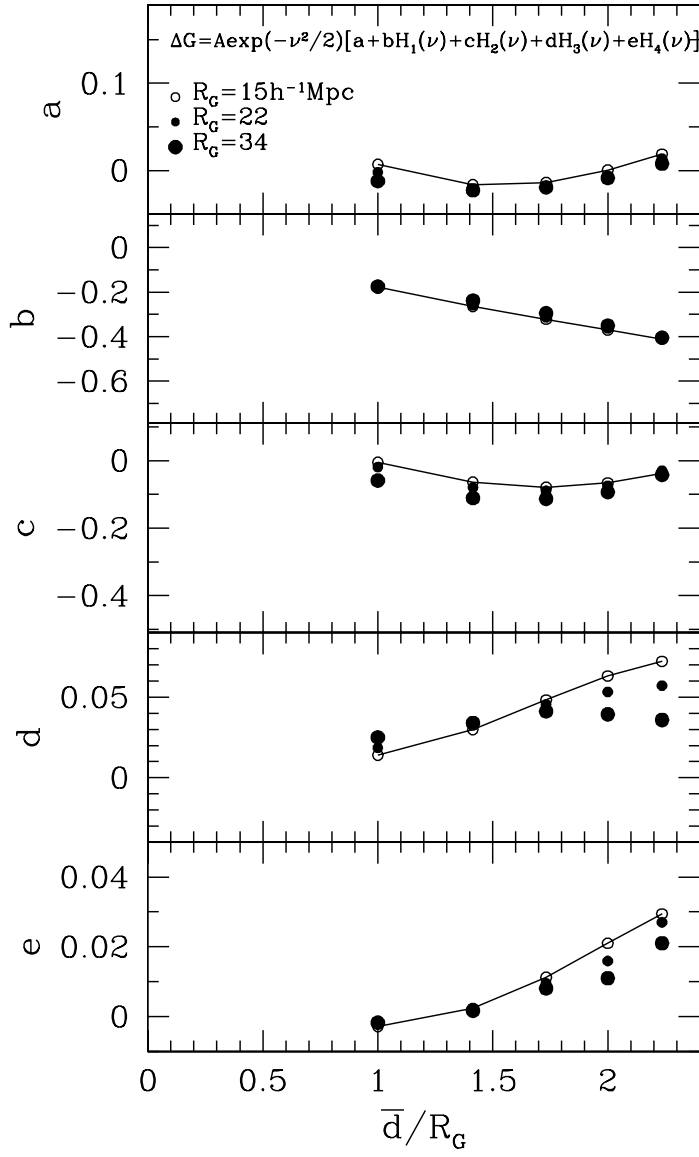


Fig. 13.— Same as Figure 11, but for halo density fields.

as  $\bar{d}/R_G$  increases, and the corresponding terms,  $cH_2$  and  $dH_3$ , are dominating the genus deviations for  $R_G = 15h^{-1}\text{Mpc}$ .

Secondly, we measure the combined effects of shot noise and halo biasing. By varying mass cut, we prepare three halo samples having the mean separations of  $\bar{d}_h = 15, 22,$  and  $34 h^{-1}\text{Mpc}$ . The mass cut of each sample in units of  $h^{-1}M_\odot$  is  $10^{13.21}, 10^{13.67},$  and  $10^{14.03}$ , respectively.

As a result the sparser halo sample has more massive halos that are more biased. We chose to vary the low mass cut to make samples with different number density because most observations yield a galaxy redshift sample with a faint flux limit or low mass limit.

From each halo sample, we make four lower-density subsamples by randomly selecting halos so that the mean halo separation becomes  $\bar{d}/R_G = 1, \sqrt{2}, \sqrt{3}, 2,$  and  $\sqrt{5}$ . For example, the halo sample with  $\bar{d}_h = 15h^{-1}\text{Mpc}$  is smoothed over  $R_G = 15h^{-1}\text{Mpc}$ , and so are its sparser subsamples with  $\bar{d}_h = \sqrt{2}, \sqrt{3}, 2,$  and  $\sqrt{5}$  times  $R_G$ . In Table 8 in Appendix A, the genus values are given as a function of  $\nu$ .

In the bottom panel of Figure 9, we show the genus curves of halos for  $\bar{d}/R_G = 1$  (solid) and  $\bar{d}/R_G = \sqrt{5}$  (dashed lines). The overall amplitude change is smaller than the matter case, but the shift and asymmetrical change in high and low density regions show the same pattern.

To measure the combined effects we calculate the difference of the genus curve between the halo and matter density fields

$$\Delta G_{\text{h,shot}}(\nu, \bar{d}/R_G) = G_{\text{h}}(\nu, \bar{d}/R_G) - G_{\text{m}}(\nu, \bar{d}/R_G = 0), \quad (14)$$

where  $G_{\text{h}}$  and  $G_{\text{m}}$  are the halo and matter genus curves, respectively. We use an approximation that  $G_{\text{m}}(\nu, \bar{d}/R_G = 0) \approx G_{\text{m}}(\nu, \bar{d}/R_G = 0.08)$ . The difference gives us the change of the genus curve due to the combined effects of the shot noise and halo bias with respect to the true matter genus curve. We use Equation (13) again to fit the deviations.

In Figure 12 we show the measured genus deviations (black lines) as well as the best-fit models (red lines). It can be seen that Equation (13) can fit the measurements extremely well again. Figure 13 shows the variation of the fitting coefficients as a function of  $\bar{d}/R_G$ . Unlike the case of the matter genus curve the coefficients  $a, c, d,$  and  $e$  are all rather small, and the only significant contribution comes from the  $bH_1$  term when  $\bar{d}/R_G = 1$  (This is the most frequently used choice for the smoothing length in the study of the genus topology [*i.e.* Park et al. 2005; Choi et al. 2010]). The coefficient  $b$  is nearly independent of the halo mass cut, and depends on  $\bar{d}/R_G$  linearly. Due to the term  $bH_1$  the genus curve is shifted to the negative  $\nu$ 's near the median threshold level. This is the meat-ball shift for biased

objects found by Park & Gott (1991, Fig. 1). The same term also produces an asymmetry of the genus curve between the high and low density thresholds (Park & Gott 1991; Park et al. 2005).

Figure 13 suggests that the combined effects of shot noise and halo bias can be estimated from the data itself because one can measure the slope of the linear relation between the coefficient  $b$  and  $\bar{d}/R_G$  using the genus curve obtained for  $\bar{d}/R_G = 1$  and the condition that  $b = 0$  at  $\bar{d}/R_G = 0$ .

## 5. Summary and Conclusions

Removing the systematic effects in the genus curve measured from the observational samples is critically important in the genus topology analysis. Application of the topology analysis in cosmology and galaxy formation such as testing non-Gaussianity of the primordial density fluctuations, constraining the expansion history of the universe, and understanding the formation and evolution of LSS will be successful only after the systematic effects accurately estimated from carefully made mock samples are subtracted from the raw data.

Using one of the currently largest cosmological N-body simulations, the HR2, we accurately measured various systematic effects on the genus statistic. The systematic effects considered are those of finite pixel size, nonlinear gravitational evolution, redshift-space distortion, shot noise or finite sampling, dark matter halo bias. It is found that all of them can be very accurately modeled with a combination of a few low-order Hermite polynomials as follows:

$$\begin{aligned}
 \Delta G_{\text{pixel}}(\nu) &= Ae^{-\nu^2/2} \times \\
 &\quad [aH_0(\nu) + bH_1(\nu) + cH_2(\nu) + dH_4(\nu)]p^2/R_G^2 \\
 \Delta G_{\text{grav}}(\nu) &= Ae^{-\nu^2/2} \times \\
 &\quad [(bH_1(\nu) + dH_3(\nu))\sigma_0 + (aH_0(\nu) + cH_2(\nu))\sigma_0^2] \\
 \Delta G_{\text{RSD}}(\nu) &= Ae^{-\nu^2/2} \times \\
 &\quad [aH_0(\nu) + bH_1(\nu) + cH_2(\nu) + dH_3(\nu)] \\
 \Delta G_{\text{h,shot}}(\nu) &= Ae^{-\nu^2/2} \times \\
 &\quad [aH_0(\nu) + bH_1(\nu) + cH_2(\nu) + dH_3(\nu) + eH_4(\nu)]
 \end{aligned}$$

where  $A$  is the amplitude of the genus curve for a Gaussian field with the measured  $\sigma_0$  and  $\sigma_1$ ,  $p$  is the pixel size, and  $R_G$  is the Gaussian smoothing length. The first three effects make the genus amplitude decrease, but the shot noise, on the other hand, increases it. The

halo bias mainly makes the genus curve shifted toward the low-density thresholds without changing the amplitude.

In the pixel effects we find that inclusion of the odd term  $H_1$  in addition to  $H_0, H_2$ , and  $H_4$  terms, as suggested by Hamilton et al. (1986), gives a better fit to the genus deviations. Figure 2 shows that the pixel size effects should be taken into account in many topology analyses in order to achieve percent-level accuracy. Weinberg et al. (1987) has suggested to use a pixel size equal to or smaller than  $p = \lambda/2.5 = \sqrt{2}R_G/2.5$ , and many follow-up studies adopted this choice. This choice of pixel size corresponds to the green line in the top panel of Figure 3 when  $R_G = 15 h^{-1}\text{Mpc}$ . The figure indicates that the amplitude drop due to the pixel effect amounts nearly 5%. It is desirable to use  $p < R_G/3$  and correct the genus curve for the remaining pixel effects.

A critical shortcoming of the second-order perturbation theory for the non-linear gravitational evolution effects is the fact that it does not predict the amplitude drop of the genus curve, which has long been known from many numerical studies (Melott et al. 1988; Park & Gott 1991; Vegeley et al. 1994; Springel et al. 1998; Park et al. 2005; Choi et al. 2010). We have found that it is the second order term  $\sigma_0^2$  in the expansion of the genus deviation with the coefficients proportional to  $H_0$  and  $H_2$  that are responsible for the amplitude drop of the genus curve (see Figs. 5 and 6). Therefore, it is necessary to extend the perturbation theory to higher orders so that the genus deviation can be expanded at least up to the second order in  $\sigma_0$ .

The dominant term of the redshift-space distortion effects is the term proportional to  $H_2$  as suggested by Matsubara (1996) from the linear perturbation theory, and the resulting main systematic effect is a decrease in the amplitude of the genus curve. The amount of the decrease depends on the growth factor and the degree of galaxy bias (Eqs. 9 and 10). We find that the  $H_2$  term is indeed dominant on the smoothing scale of  $R_G = 34 h^{-1}\text{Mpc}$  but that the genus deviation should be modeled with additional terms such as  $H_0, H_1$ , and  $H_3$  on smaller scales. The redshift-space distortion effects make the cluster abundance decrease more than the void abundance (Figs. 7 and 8). On those scales, it is also expected that the coefficient of  $H_2$  is different from the analytic prediction because the galaxy or halo bias is not exactly linear and constant as assumed in the linear perturbation theory (Jee et al. 2012).

The shot noise in the smoothed density field reconstructed from a galaxy catalog gives the biggest effects on the genus curve and must be very accurately estimated. Figures 9 and 10 show that the shot noise characteristically makes the amplitude of the genus curve increase by making the density field choppier, shifts the curve near the median level to the left (the meat-ball shift), and increases the cluster abundance by breaking up high-density

regions. The void abundance is relatively much less affected.

The shot noise effects diminish greatly when biased objects are used. The effects become much smaller when the subsample is constructed by making the mean halo separation equal to the smoothing length through selection of the most biased objects. Figure 12 shows that, when  $\bar{d} = R_G$ , the genus deviation is symmetric and produces a meat-ball shift in the genus curve with little change in amplitude. Considering the characteristics of the shot noise effects, we conclude that this deviation proportional to  $H_1$  (Fig. 13) is mostly due to the halo bias. The figure indicates that the optimal Gaussian smoothing length for the genus topology analysis is  $R_G = \bar{d}$ , the mean halo/galaxy separation itself. In the early studies of topology of large-scale structure the choice of  $R_G = \bar{d}/\sqrt{2}$  has been widely used (Weinberg et al. 1987; Gott et al. 1989; Vogeley et al. 1994). But  $R_G = \bar{d}$  is used in most recent analyses (Park et al. 2005; Gott et al. 2009; Choi et al. 2010, 2014).

We suggest not to use subsamples with galaxies randomly selected from the parent catalog as this greatly amplifies the shot noise effects. Instead, it is desirable to vary the luminosity or mass cut to make subsamples of galaxies. The sample used in the top panel of Figure 12 contains halos with a low mass cut that results in the mean halo separation of  $15 h^{-1}\text{Mpc}$  while the halo sample in the bottom panel has a relatively higher low mass cut giving  $\bar{d} = 34 h^{-1}\text{Mpc}$ . If we randomly remove some halos in the first sample to make the mean separation  $\sqrt{5} \times 15 h^{-1}\text{Mpc} \approx 34 h^{-1}\text{Mpc}$ , the amplitude excess due to the shot noise is about 15% at  $\nu = 0$ . On the other hand, it is about 4% for the latter sample of more massive halos.

It should be pointed out that our estimation of the systematic effects is directly useful only for the particular  $\Lambda\text{CDM}$  model we adopt and for a set of particular smoothing scales and dark halo mass cuts. When one analyzes an observational sample and compare it with a cosmological model, it is necessary to perform a detailed modeling of the observed objects in that particular cosmology and estimate all the systematic effects in the genus curve as considered in this paper. Similar studies are needed for other Minkowski functionals and Betti numbers.

The authors thank Prof. Juhan Kim for helpful comments on the paper and also for kindly providing a parallel code for computing the genus. The authors also thank Korea Institute for Advanced Study for providing computing resources (KIAS Center for Advanced Computation Linux Cluster System). Y.-Y. C was supported by the National Research Foundation of Korea to the Center for Galaxy Evolution Research. (NO. 2010-0027910). J.-E.L. was supported by the 2013 Sabbatical Leave Program of Kyung Hee University (KHU-20131724). S.S.K., J.S., and M.K.'s work was supported by the BK21 plus

program through the NRF of Korea.

### A. Genus Curves

In this appendix, we provide tables of the genus curves used in this study for the reader who wishes to study the various systematic effects on the genus curve. All the systematic effects were examined at three different smoothing lengths,  $R_G = 15, 22,$  and  $34 h^{-1}\text{Mpc}$ . Electronic versions of these tables are available from the authors upon request.

Table 3: Coefficients for redshift-space distortion effects for the matter density fields

$\Delta G_{\text{RSD}}/A = e^{-\nu^2/2}(aH_0 + bH_1 + cH_2 + dH_3)$							
$R_G$	$a$	$b$	$c$	$d$	$\Delta_{r.m.s.}$	$\sigma_0$	$\sigma_1$
15	0.0037	0.01677	0.0478	0.0068	3.6e-4	0.25947	0.01709
22	0.0017	0.00698	0.0372	0.0034	7.9e-4	0.17529	0.00825
34	0.0003	0.00098	0.0288	0.0010	15.2e-4	0.10745	0.00343

---

Note. — Smoothing length  $R_G$  is in units of  $h^{-1}\text{Mpc}$ . The smallest pixel size of  $p = 3.33 h^{-1}\text{Mpc}$  is used to minimize the pixel effect. Amplitude  $A$  is 520141, 189599, and 59084 for  $R_G = 15, 22,$  and  $34 h^{-1}\text{Mpc}$ , respectively.  $\Delta_{r.m.s.}$  is calculated from  $\sqrt{\sum_{j=1}^N \frac{1}{N} [\Delta G_{\text{RSD}}^{\text{sim}}(\nu_j)/A - \Delta G_{\text{RSD}}(\nu_j)/A]^2}$  where  $\Delta G_{\text{RSD}}^{\text{sim}}(\nu_j)$  is from simulation and  $\Delta G_{\text{RSD}}(\nu)$  is the best-fit function.





Table 4—Continued

$\nu$	$p = 3.33$	3.75	4	5	5.71	6	6.67	7.5	8	8.57	10	12
-1.5	-72758	-72617	-72563	-72266	-72060	-72032	-71810	-71406	-71216	-71031	-70047	-69023
-1.4	-64189	-64196	-64172	-63943	-63876	-63753	-63607	-63340	-63221	-62958	-62439	-61352
-1.3	-52371	-52335	-52340	-52220	-52152	-52209	-52020	-51866	-51668	-51470	-51106	-50631
-1.2	-37173	-37159	-37070	-37031	-36991	-37026	-37146	-36938	-37000	-36865	-36675	-36526
-1.1	-18771	-18749	-18730	-18824	-18813	-18878	-18885	-18961	-18960	-18902	-19003	-19282
-1.0	2204	2208	2173	2074	1942	1885	1794	1570	1379	1139	953	289
-0.9	25406	25328	25284	25177	25073	24915	24775	24548	24313	24153	23582	22601
-0.8	49929	49839	49847	49485	49234	49163	48908	48493	48169	47975	47115	45746
-0.7	75260	75146	75066	74624	74281	74172	73796	73367	73018	72772	71604	70031
-0.6	100192	100030	99987	99524	99227	99096	98659	98054	97636	97071	95949	94122
-0.5	123912	123767	123651	123154	122814	122529	122070	121310	121110	120494	118955	116389
-0.4	145023	144812	144733	144115	143660	143435	142861	142166	141751	141116	139624	136978
-0.3	161794	161612	161472	160928	160339	160168	159619	158898	158337	157864	156000	153285
-0.2	174460	174217	174054	173555	172968	172847	172255	171366	170779	170133	168692	165819
-0.1	181982	181705	181661	180963	180481	180264	179676	178830	178335	177936	175927	173193
0.0	184278	184128	184058	183450	182948	182613	182101	181341	180770	180137	178249	175716
0.1	181546	181294	181192	180622	180169	179984	179356	178689	178006	177522	175790	172913
0.2	173054	172883	172786	172281	171843	171506	171066	170329	169785	169295	167601	164929
0.3	159963	159809	159660	159123	158679	158401	157976	157181	156669	156047	154574	151864
0.4	142114	141989	141773	141449	140923	140808	140249	139600	139188	138714	137282	134864
0.5	120685	120481	120426	119995	119733	119538	119128	118508	118092	117696	116523	114276
0.6	96707	96524	96500	96166	95875	95707	95462	94740	94702	94478	93168	91474
0.7	71154	71151	71122	70856	70514	70536	70157	69872	69741	69244	68505	67425
0.8	44985	44965	44929	44749	44482	44528	44411	44156	44044	43806	43201	42194
0.9	19694	19665	19681	19594	19583	19539	19438	19368	19261	19056	18797	18012
1.0	-4038	-4091	-4091	-4091	-4098	-4073	-4319	-4106	-4196	-4388	-4429	-4571
1.1	-25481	-25488	-25481	-25357	-25291	-25317	-25374	-25064	-25145	-25117	-24814	-24452
1.2	-43670	-43612	-43590	-43402	-43295	-43238	-43216	-42889	-42791	-42676	-42260	-41623
1.3	-59174	-59082	-59016	-58808	-58639	-58470	-58346	-58010	-57907	-57440	-56818	-55855
1.4	-70850	-70808	-70643	-70459	-70086	-69985	-69729	-69392	-69116	-68765	-67976	-66628
1.5	-78835	-78741	-78688	-78332	-78068	-77951	-77626	-77202	-76929	-76561	-75633	-74110
1.6	-83970	-83840	-83763	-83355	-83056	-82922	-82586	-82053	-81714	-81329	-80195	-78224
1.7	-85950	-85854	-85771	-85403	-85001	-84877	-84469	-83802	-83481	-83085	-81853	-79851
1.8	-85257	-85100	-84916	-84522	-84031	-83932	-83500	-83014	-82500	-82043	-80781	-78838
1.9	-82259	-82127	-81952	-81527	-81033	-80941	-80585	-79952	-79548	-79125	-77885	-75789
2.0	-77367	-77233	-77059	-76686	-76245	-76094	-75661	-74975	-74738	-74271	-73048	-71042
2.1	-71645	-71466	-71405	-70968	-70573	-70402	-69989	-69508	-69102	-68625	-67439	-65367
2.2	-64801	-64680	-64594	-64159	-63878	-63651	-63268	-62698	-62404	-61892	-60656	-58838
2.3	-57654	-57518	-57437	-57079	-56784	-56612	-56156	-55743	-55372	-55092	-53916	-52285
2.4	-50693	-50593	-50510	-50147	-49847	-49671	-49309	-48943	-48617	-48293	-47224	-45751
2.5	-43807	-43704	-43652	-43326	-43067	-42918	-42646	-42195	-41930	-41587	-40620	-39232

$R_G = 34 \text{ h}^{-1} \text{Mpc}$												
-2.5	-13250	-13225	-13226	-13182	-13179	-13153	-13108	-13059	-13009	-12945	-12818	-12622
-2.4	-15377	-15357	-15371	-15318	-15267	-15270	-15216	-15163	-15133	-15077	-14957	-14757
-2.3	-17462	-17445	-17430	-17365	-17327	-17329	-17290	-17222	-17183	-17135	-17014	-16792
-2.2	-19491	-19473	-19477	-19417	-19350	-19348	-19314	-19234	-19213	-19163	-18973	-18743
-2.1	-21464	-21457	-21430	-21410	-21346	-21328	-21305	-21237	-21189	-21122	-21004	-20766
-2.0	-23147	-23116	-23101	-23020	-22990	-22952	-22925	-22846	-22800	-22739	-22556	-22306
-1.9	-24485	-24479	-24472	-24395	-24332	-24323	-24278	-24219	-24158	-24100	-23963	-23722
-1.8	-25212	-25201	-25191	-25118	-25089	-25058	-25002	-24936	-24837	-24814	-24660	-24438
-1.7	-25175	-25171	-25158	-25111	-25050	-25038	-25006	-24921	-24897	-24870	-24738	-24455
-1.6	-24390	-24383	-24362	-24357	-24347	-24325	-24303	-24233	-24179	-24132	-24038	-23903
-1.5	-22789	-22786	-22789	-22740	-22685	-22704	-22636	-22595	-22628	-22546	-22498	-22308
-1.4	-20156	-20155	-20147	-20128	-20107	-20144	-20115	-20083	-20035	-20042	-19932	-19801
-1.3	-16294	-16311	-16276	-16268	-16287	-16269	-16210	-16193	-16232	-16239	-16203	-16177
-1.2	-11414	-11407	-11421	-11399	-11405	-11426	-11396	-11411	-11386	-11322	-11355	-11271
-1.1	-5758	-5753	-5803	-5761	-5730	-5753	-5734	-5720	-5770	-5744	-5871	-5850
-1.0	890	877	862	847	865	898	833	801	757	761	715	717
-0.9	8114	8122	8143	8114	8093	8121	8070	8039	8001	8022	7892	7767
-0.8	15838	15828	15819	15744	15762	15752	15757	15642	15620	15704	15534	15343
-0.7	23770	23789	23749	23692	23675	23631	23562	23503	23497	23453	23260	23066
-0.6	31735	31711	31694	31643	31593	31584	31517	31446	31444	31355	31178	30902
-0.5	39136	39116	39117	39030	38992	38945	38896	38893	38792	38775	38623	38302
-0.4	45995	45947	45920	45848	45790	45733	45710	45608	45586	45525	45331	45068
-0.3	51434	51410	51392	51328	51258	51235	51161	51029	51026	50912	50737	50289

Table 4—Continued

$\nu$	$p = 3.33$	3.75	4	5	5.71	6	6.67	7.5	8	8.57	10	12
-0.2	55378	55370	55368	55244	55215	55175	55093	55012	54945	54848	54653	54304
-0.1	57771	57734	57709	57638	57560	57524	57439	57354	57279	57147	56962	56532
0.0	58438	58435	58403	58344	58263	58269	58172	58089	58059	57948	57802	57383
0.1	57578	57538	57497	57407	57369	57329	57273	57146	57110	56973	56803	56494
0.2	54826	54796	54799	54714	54650	54689	54555	54518	54400	54340	54108	53789
0.3	50461	50429	50446	50353	50315	50285	50220	50125	50046	49940	49775	49475
0.4	44616	44592	44591	44533	44445	44423	44371	44308	44241	44157	43942	43652
0.5	37705	37691	37721	37608	37530	37515	37510	37388	37370	37332	37144	36763
0.6	30136	30124	30113	30089	30042	30032	29973	29892	29911	29881	29740	29537
0.7	22292	22289	22274	22242	22187	22176	22107	22115	22043	22029	21898	21616
0.8	14091	14103	14103	14021	14043	13995	13994	13984	13947	13938	13826	13610
0.9	6205	6193	6224	6166	6117	6199	6148	6136	6146	6106	6081	5979
1.0	-1353	-1354	-1358	-1323	-1399	-1347	-1442	-1425	-1433	-1428	-1493	-1455
1.1	-7988	-7997	-7997	-7997	-8006	-7973	-8026	-7987	-8013	-7984	-7942	-7997
1.2	-13831	-13815	-13801	-13777	-13819	-13777	-13748	-13762	-13744	-13726	-13773	-13738
1.3	-18649	-18639	-18629	-18607	-18600	-18574	-18543	-18517	-18545	-18424	-18390	-18267
1.4	-22263	-22266	-22237	-22216	-22189	-22152	-22111	-22030	-22010	-22021	-21826	-21672
1.5	-24713	-24707	-24698	-24631	-24635	-24607	-24563	-24501	-24495	-24430	-24312	-24115
1.6	-26366	-26339	-26323	-26306	-26277	-26233	-26180	-26145	-26125	-26058	-25907	-25612
1.7	-26923	-26892	-26888	-26824	-26800	-26773	-26721	-26637	-26629	-26525	-26395	-26180
1.8	-26776	-26754	-26736	-26658	-26598	-26588	-26512	-26465	-26373	-26314	-26152	-25906
1.9	-25838	-25817	-25804	-25725	-25670	-25673	-25596	-25525	-25441	-25428	-25229	-24929
2.0	-24369	-24352	-24343	-24259	-24207	-24197	-24117	-24034	-23981	-23918	-23721	-23380
2.1	-22425	-22384	-22379	-22310	-22231	-22208	-22157	-22072	-22009	-21941	-21814	-21523
2.2	-20325	-20308	-20281	-20229	-20193	-20133	-20116	-20032	-19967	-19906	-19747	-19471
2.3	-18180	-18167	-18130	-18096	-18072	-18012	-18006	-17908	-17849	-17791	-17643	-17426
2.4	-16031	-16015	-15996	-15946	-15905	-15866	-15856	-15759	-15721	-15644	-15497	-15287
2.5	-13815	-13805	-13806	-13749	-13696	-13699	-13626	-13585	-13544	-13498	-13317	-13123

Note. — Genus values at a given threshold level of the density field estimated from a discrete particle distribution. The density field was smoothed with smoothing length  $R_G = 15 h^{-1}\text{Mpc}$ . We use a set of grids with cubic pixels and with size of 2160, 1920, 1800, 1440, 1260, 1200, 1080, 960, 900, 840, 720, and 600 in terms of number of pixels along a side. Since the physical size of HR2 is  $7200 h^{-1}\text{Mpc}$ , they correspond to 3.33, 3.75, 4, 5, 5.71, 6, 6.67, 7.5, 8, 8.57, 10, and 12  $h^{-1}\text{Mpc}$ , respectively, in terms of pixel size  $p$ .

Table 5: Genus values at a Given Threshold Level for the Matter Density Field Samples Used to Estimate the Non-linear Gravitational Evolution Effects

$\nu$	$R_G = 15h^{-1}\text{Mpc}$		$R_G = 22h^{-1}\text{Mpc}$		$R_G = 34h^{-1}\text{Mpc}$	
	$G_{m,r} _{z=32}$	$G_{m,r} _{z=0}$	$G_{m,r} _{z=32}$	$G_{m,r} _{z=0}$	$G_{m,r} _{z=32}$	$G_{m,r} _{z=0}$
-2.5	-108992	-116313	-41134	-43267	-13250	-13683
-2.4	-126596	-135266	-47665	-50342	-15377	-15901
-2.3	-144775	-154571	-54593	-57606	-17462	-18078
-2.2	-162787	-173653	-61261	-64555	-19491	-20234
-2.1	-179620	-190606	-67562	-71101	-21464	-22285
-2.0	-193867	-206042	-73024	-76917	-23147	-24115
-1.9	-205228	-218159	-77381	-81628	-24485	-25448
-1.8	-212676	-225541	-79818	-84236	-25212	-26240
-1.7	-214571	-226813	-80154	-84723	-25175	-26353
-1.6	-209091	-220701	-77793	-82486	-24390	-25706
-1.5	-195988	-207088	-72758	-77269	-22789	-23980
-1.4	-174461	-184193	-64189	-68525	-20156	-21381
-1.3	-143570	-151186	-52371	-56390	-16294	-17438
-1.2	-103593	-109502	-37173	-40876	-11414	-12575
-1.1	-56058	-58746	-18771	-21605	-5758	-6745
-1.0	-407	-307	2204	-104	890	-68
-0.9	60985	64655	25406	23958	8114	7232
-0.8	126949	133567	49929	49094	15838	15138
-0.7	194587	203207	75260	75396	23770	23416
-0.6	260604	272365	100192	101707	31735	31371
-0.5	323216	337302	123912	125978	39136	39205
-0.4	378505	395286	145023	147247	45995	46214
-0.3	425471	444378	161794	164908	51434	51848
-0.2	460367	480671	174460	178298	55378	56050
-0.1	483040	503357	181982	186729	57771	58542
0.0	490296	510839	184278	190051	58438	59482
0.1	482916	503491	181546	186997	57578	58662
0.2	461376	480720	173054	178788	54826	56074
0.3	426492	444352	159963	165242	50461	51751
0.4	379352	395592	142114	147385	44616	45881
0.5	323075	337400	120685	125919	37705	38921
0.6	260303	272285	96707	101880	30136	31760
0.7	192725	203385	71154	75822	22292	23580
0.8	124309	132825	44985	49176	14091	15239
0.9	57185	64125	19694	23616	6205	7355
1.0	-6323	-644	-4038	-487	-1353	-176
1.1	-63409	-59764	-25481	-22161	-7988	-6988
1.2	-113185	-109888	-43670	-41073	-13831	-12873
1.3	-153819	-151472	-59174	-56711	-18649	-17694
1.4	-186058	-183899	-70850	-68593	-22263	-21514
1.5	-208250	-207196	-78835	-77001	-24713	-23963
1.6	-221960	-220977	-83970	-82376	-26366	-25744
1.7	-227736	-226528	-85950	-84319	-26923	-26298
1.8	-226079	-224735	-85257	-83785	-26776	-26311
1.9	-218582	-217560	-82259	-81045	-25838	-25425
2.0	-206241	-205534	-77367	-76353	-24369	-23956
2.1	-190950	-190078	-71645	-70656	-22425	-22139
2.2	-173112	-172168	-64801	-64083	-20325	-20044
2.3	-153979	-152990	-57654	-57118	-18180	-18030
2.4	-134751	-133959	-50693	-50169	-16031	-15874
2.5	-116288	-115788	-43807	-43408	-13815	-13697

Note. —  $G_{m,r}|_{z=32}$  and  $G_{m,r}|_{z=0}$  are real-space genus values of the dark matter distributions at initial epoch of the simulation ( $z = 32$ ) and at final epoch ( $z = 0$ ), respectively, using a large array of  $2160^3$  pixels ( $p = 3.33 h^{-1}\text{Mpc}$ ).

Table 6: Genus Values at a Given Threshold Level for the Samples Used to Estimate the Redshift-space Distortion Effects

$\nu$	Matter						Halo					
	$R_G = 15h^{-1}\text{Mpc}$		$R_G = 22h^{-1}\text{Mpc}$		$R_G = 34h^{-1}\text{Mpc}$		$R_G = 15h^{-1}\text{Mpc}$		$R_G = 22h^{-1}\text{Mpc}$		$R_G = 34h^{-1}\text{Mpc}$	
	$G_{m,r}$	$G_{m,z}$	$G_{m,r}$	$G_{m,z}$	$G_{m,r}$	$G_{m,z}$	$G_{h,r}$	$G_{h,z}$	$G_{h,r}$	$G_{h,z}$	$G_{h,r}$	$G_{h,z}$
-2.5	-116313	-105435	-43267	-39876	-13683	-12876	-102261	-99669	-39240	-38419	-13003	-12745
-2.4	-135266	-122203	-50342	-46292	-15901	-14877	-117627	-114673	-45125	-44111	-14855	-14558
-2.3	-154571	-139699	-57606	-52889	-18078	-16884	-132824	-129274	-50919	-49625	-16752	-16548
-2.2	-173653	-156927	-64555	-59259	-20234	-18913	-147195	-143294	-56411	-55188	-18574	-18282
-2.1	-190606	-173381	-71101	-65410	-22285	-20856	-160452	-156276	-61145	-59716	-20149	-19871
-2.0	-206042	-187213	-76917	-70613	-24115	-22577	-170947	-166189	-64882	-63491	-21432	-21074
-1.9	-218159	-197904	-81628	-74642	-25448	-23660	-177276	-172432	-67059	-65851	-22160	-21855
-1.8	-225541	-204475	-84236	-77105	-26240	-24384	-179216	-174259	-67728	-66217	-22333	-21948
-1.7	-226813	-205789	-84723	-77466	-26353	-24505	-174754	-170281	-65966	-64347	-21698	-21373
-1.6	-220701	-200599	-82486	-75297	-25706	-23864	-163768	-159279	-61641	-60027	-20253	-19902
-1.5	-207088	-188090	-77269	-70301	-23980	-22100	-145480	-141253	-54512	-53030	-17983	-17760
-1.4	-184193	-167012	-68525	-62021	-21381	-19444	-118359	-115328	-44231	-43271	-14680	-14394
-1.3	-151186	-137667	-56390	-50503	-17438	-15984	-83337	-80739	-30665	-29771	-10304	-10157
-1.2	-109502	-99820	-40876	-35688	-12575	-11067	-39293	-38560	-14141	-13600	-5102	-4975
-1.1	-58746	-53195	-21605	-18061	-6745	-5385	10781	10990	5592	5403	1005	1191
-1.0	-307	-289	-104	2390	-68	1054	67923	66761	27243	26872	8260	8226
-0.9	64655	58683	23958	24762	7232	8123	129579	126265	50801	50347	15829	15854
-0.8	133567	121533	49094	48751	15138	15507	194007	189367	75305	73879	23590	23388
-0.7	203207	186681	75396	73429	23416	23154	258434	251997	99154	97575	31563	31110
-0.6	272365	248968	101707	97331	31371	30880	319970	311566	121886	120025	38994	38468
-0.5	337302	308522	125978	119804	39205	38090	375748	366234	142869	140126	45453	45045
-0.4	395286	361770	147247	139414	46214	44521	423008	412037	160525	157737	51101	50594
-0.3	444378	406444	164908	155752	51848	49977	459398	447844	174053	171113	55801	54976
-0.2	480671	439533	178298	168028	56050	53761	484631	472590	182765	179387	58512	57823
-0.1	503357	460455	186729	175348	58542	56116	495940	483765	186476	182929	59865	59131
0.0	510839	467357	190051	177809	59482	56827	492597	479888	184577	181032	59107	58348
0.1	503491	460428	186997	174608	58662	55971	473891	461746	177239	173748	56758	56031
0.2	480720	439595	178788	166731	56074	53274	441327	430011	164478	161223	52722	52003
0.3	444352	406600	165242	154089	51751	49126	394982	385197	146916	144258	46948	46315
0.4	395592	361476	147385	136789	45881	43455	340326	331818	125546	123116	39850	39431
0.5	337400	308017	125919	116257	38921	36614	277462	269690	101133	99298	32045	31555
0.6	272285	247690	101880	93354	31760	29220	208490	202517	74849	73390	23701	23321
0.7	203385	184505	75822	68442	23580	21473	136121	132933	47330	46327	14891	14660
0.8	132825	119637	49176	43495	15239	13514	64902	63549	20326	19869	6462	6305
0.9	64125	55910	23616	18879	7355	5810	-3867	-2808	-5355	-5415	-1960	-1874
1.0	-644	-4157	-487	-4042	-176	-1369	-66799	-65007	-28645	-28365	-9337	-9346
1.1	-59764	-58193	-22161	-24271	-6988	-7838	-122715	-119034	-49424	-48931	-15834	-15720
1.2	-109888	-104589	-41073	-41814	-12873	-13565	-170334	-164877	-67092	-65886	-21350	-21214
1.3	-151472	-143835	-56711	-56487	-17694	-18231	-207441	-201443	-80908	-79406	-25789	-25545
1.4	-183899	-173656	-68593	-67831	-21514	-21736	-235223	-228670	-90900	-89482	-28871	-28728
1.5	-207196	-194941	-77001	-75753	-23963	-24046	-252821	-246087	-97174	-95306	-31018	-30740
1.6	-220977	-207743	-82376	-80344	-25744	-25614	-261786	-254261	-100085	-98463	-31873	-31574
1.7	-226528	-212588	-84319	-82188	-26298	-26047	-262781	-255334	-100080	-98410	-31775	-31534
1.8	-224735	-210939	-83785	-81382	-26311	-25910	-256944	-249623	-97305	-95670	-31079	-30688
1.9	-217560	-20000	-81045	-78645	-25425	-25009	-245387	-238300	-92841	-91152	-29580	-29273
2.0	-205534	-192481	-76353	-74198	-23956	-23591	-228725	-222284	-86288	-84666	-27555	-27282
2.1	-190078	-178068	-70656	-68258	-22139	-21790	-209709	-203700	-78719	-77300	-25177	-24899
2.2	-172168	-161285	-64083	-61821	-20044	-19774	-188317	-182962	-70751	-69411	-22541	-22399
2.3	-152990	-143461	-57118	-55137	-18030	-17615	-166473	-161865	-62751	-61617	-19915	-19663
2.4	-133959	-125628	-50169	-48402	-15874	-15474	-144722	-140654	-54656	-53737	-17405	-17220
2.5	-115788	-108441	-43408	-41751	-13697	-13353	-124021	-120785	-46823	-45995	-14957	-14800

Note. —  $G_{m,r}$  and  $G_{m,z}$  are genus values of dark matter density fields in redshift space and real space at  $z = 0$ , respectively.  $G_{h,r}$  and  $G_{h,z}$  are genus values of halo density fields in redshift space and real space at  $z = 0$ , respectively. A large array of  $2160^3$  pixels ( $p = 3.33 h^{-1}\text{Mpc}$ ) is used.

Table 7. Genus Values at a Given Threshold Level for the Samples to Estimate the Effects of Shot Noise in the Matter Density Field

$\nu$	$\bar{d}/R_G = 0.08$	0.16	0.32	0.64	1.0	$\sqrt{2}$	$\sqrt{3}$	2.0	$\sqrt{5}$
$R_G = 15 h^{-1}\text{Mpc}$									
-2.5	-108803	-109097	-110747	-120821	-140353	-154544	-152069	-140914	-129580
-2.4	-126479	-126635	-128280	-140073	-161425	-178082	-175107	-162247	-148798
-2.3	-144533	-144903	-146578	-158972	-182971	-202184	-198173	-183704	-167654
-2.2	-162671	-162865	-164723	-178013	-203321	-224608	-220301	-204104	-186106
-2.1	-179447	-179682	-181609	-195462	-222438	-245411	-240344	-222120	-201790
-2.0	-193774	-194052	-196385	-210250	-238326	-261728	-256636	-235974	-213593
-1.9	-205192	-205588	-207647	-221167	-249510	-272704	-267465	-245113	-220938
-1.8	-212516	-212808	-214623	-227601	-254942	-276779	-270455	-246928	-220084
-1.7	-214418	-214488	-215837	-228118	-253665	-271836	-264220	-239035	-211509
-1.6	-208895	-208873	-210525	-220441	-242145	-256844	-246865	-220657	-192357
-1.5	-195759	-195714	-197125	-204527	-220545	-230384	-216905	-190261	-161745
-1.4	-174307	-174532	-175099	-179766	-189677	-191601	-174263	-146521	-118847
-1.3	-143465	-143340	-143716	-145065	-146893	-140741	-119294	-90084	-63894
-1.2	-103662	-103518	-103184	-101097	-94008	-76548	-50740	-20089	4722
-1.1	-56031	-55991	-54581	-47947	-31315	-2501	28810	61627	84663
-1.0	-503	-519	1661	12767	40229	81058	118224	153571	174303
-0.9	60775	61199	63872	79433	118138	171146	214279	252995	272179
-0.8	126761	127474	130070	149998	198890	264895	313851	358777	375211
-0.7	194422	194879	197663	221578	279988	358710	413485	460638	477452
-0.6	260443	261029	264630	292040	358638	449167	508048	557504	575569
-0.5	322939	323275	327086	358595	430979	531361	594576	644719	664937
-0.4	378167	378349	383541	416462	493846	601666	669233	718003	736801
-0.3	425068	425911	430474	462874	544638	655540	726074	772234	792788
-0.2	460248	461023	465314	498348	580280	692958	762495	806075	833702
-0.1	482725	483160	486930	519289	598023	709078	776693	817687	851076
0.0	490162	490602	494963	524479	599075	704346	768197	805065	839598
0.1	482659	483270	486690	513908	582957	677895	737392	769167	801019
0.2	461251	461386	465121	488200	548823	633128	683867	711796	738378
0.3	426363	426333	429141	448002	499130	569389	611928	633861	652975
0.4	379233	379263	381873	396700	436841	491824	524140	540298	552158
0.5	322841	323181	324791	335245	363431	403392	425264	435647	437450
0.6	260225	260348	261250	267166	282856	307069	319402	322174	315898
0.7	192897	192901	193653	195594	200500	207587	209686	204974	192795
0.8	124318	124534	124193	122231	116915	110098	101429	90069	72889
0.9	56915	56629	55862	51428	37036	16423	-2675	-19102	-39319
1.0	-6521	-6545	-8008	-15212	-37125	-70316	-96892	-118535	-139294
1.1	-63131	-63701	-64788	-75217	-102750	-145860	-180410	-205552	-226705
1.2	-113080	-113102	-114836	-126726	-158058	-209987	-249572	-278323	-301021
1.3	-153644	-154289	-156083	-169290	-203187	-260274	-303650	-335258	-359262
1.4	-185906	-185649	-187593	-201015	-237710	-297518	-342879	-376007	-400979
1.5	-208150	-208352	-209985	-223703	-260458	-321559	-368248	-401699	-426925
1.6	-221915	-222178	-223476	-236510	-272425	-333810	-379409	-412845	-438066
1.7	-227557	-227578	-229451	-241591	-275986	-334481	-379473	-411791	-435412
1.8	-225816	-225698	-227421	-239490	-271383	-326114	-368835	-399876	-422136
1.9	-218403	-218343	-219950	-230627	-259817	-310545	-350630	-378792	-399210
2.0	-205990	-206152	-207552	-217543	-243245	-289090	-326096	-352110	-370887
2.1	-190671	-190841	-191736	-200667	-223458	-264538	-297114	-321526	-337949
2.2	-172966	-173058	-173890	-181509	-201590	-237259	-265725	-287890	-301764
2.3	-153895	-154013	-154748	-161439	-178603	-209352	-233754	-252854	-265216
2.4	-134555	-134694	-135611	-141081	-155689	-181824	-202628	-218861	-229496
2.5	-116095	-116228	-116613	-121666	-133372	-155784	-172944	-186684	-195217
$R_G = 22 h^{-1}\text{Mpc}$									
-2.5	-40688	-109097	-110747	-120821	-140353	-154544	-152069	-140914	-129580
-2.4	-47089	-126635	-128280	-140073	-161425	-178082	-175107	-162247	-148798
-2.3	-53783	-144903	-146578	-158972	-182971	-202184	-198173	-183704	-167654
-2.2	-60464	-162865	-164723	-178013	-203321	-224608	-220301	-204104	-186106
-2.1	-66691	-179682	-181609	-195462	-222438	-245411	-240344	-222120	-201790
-2.0	-72159	-194052	-196385	-210250	-238326	-261728	-256636	-235974	-213593
-1.9	-76305	-205588	-207647	-221167	-249510	-272704	-267465	-245113	-220938
-1.8	-78548	-212808	-214623	-227601	-254942	-276779	-270455	-246928	-220084
-1.7	-78965	-214488	-215837	-228118	-253665	-271836	-264220	-239035	-211509
-1.6	-76721	-208873	-210525	-220441	-242145	-256844	-246865	-220657	-192357

Table 7—Continued

$\nu$	$\bar{d}/R_G = 0.08$	0.16	0.32	0.64	1.0	$\sqrt{2}$	$\sqrt{3}$	2.0	$\sqrt{5}$
-1.5	-71404	-195714	-197125	-204527	-220545	-230384	-216905	-190261	-161745
-1.4	-63360	-174532	-175099	-179766	-189677	-191601	-174263	-146521	-118847
-1.3	-51538	-143340	-143716	-145065	-146893	-140741	-119294	-90084	-63894
-1.2	-36399	-103518	-103184	-101097	-94008	-76548	-50740	-20089	4722
-1.1	-17998	-55991	-54581	-47947	-31315	-2501	28810	61627	84663
-1.0	2571	-519	1661	12767	40229	81058	118224	153571	174303
-0.9	25090	61199	63872	79433	118138	171146	214279	252995	272179
-0.8	49339	127474	130070	149998	198890	264895	313851	358777	375211
-0.7	73866	194879	197663	221578	279988	358710	413485	460638	477452
-0.6	98822	261029	264630	292040	358638	449167	508048	557504	575569
-0.5	121655	323275	327086	358595	430979	531361	594576	644719	664937
-0.4	142333	378349	383541	416462	493846	601666	669233	718003	736801
-0.3	159218	425911	430474	462874	544638	655540	726074	772234	792788
-0.2	171894	461023	465314	498348	580280	692958	762495	806075	833702
-0.1	179482	483160	486930	519289	598023	709078	776693	817687	851076
0.0	181657	490602	494963	524479	599075	704346	768197	805065	839598
0.1	178930	483270	486690	513908	582957	677895	737392	769167	801019
0.2	170814	461386	465121	488200	548823	633128	683867	711796	738378
0.3	157726	426333	429141	448002	499130	569389	611928	633861	652975
0.4	140133	379263	381873	396700	436841	491824	524140	540298	552158
0.5	119100	323181	324791	335245	363431	403392	425264	435647	437450
0.6	95226	260348	261250	267166	282856	307069	319402	322174	315898
0.7	69910	192901	193653	195594	200500	207587	209686	204974	192795
0.8	44396	124534	124193	122231	116915	110098	101429	90069	72889
0.9	19698	56629	55862	51428	37036	16423	-2675	-19102	-39319
1.0	-4087	-6545	-8008	-15212	-37125	-70316	-96892	-118535	-139294
1.1	-25061	-63701	-64788	-75217	-102750	-145860	-180410	-205552	-226705
1.2	-43207	-113102	-114836	-126726	-158058	-209987	-249572	-278323	-301021
1.3	-58281	-154289	-156083	-169290	-203187	-260274	-303650	-335258	-359262
1.4	-69736	-185649	-187593	-201015	-237710	-297518	-342879	-400107	-400979
1.5	-77986	-208352	-209985	-223703	-260458	-321559	-368248	-401699	-426925
1.6	-82798	-222178	-223476	-236510	-272425	-333810	-379409	-412845	-438066
1.7	-84849	-227578	-229451	-241591	-275986	-334481	-379473	-411791	-435412
1.8	-84219	-225698	-227421	-239490	-271383	-326114	-368835	-399876	-422136
1.9	-81147	-218343	-219950	-230627	-259817	-310545	-350630	-378792	-399210
2.0	-76466	-206152	-207552	-217543	-243245	-289090	-326096	-352110	-370887
2.1	-70787	-190841	-191736	-200667	-223458	-264538	-297114	-321526	-337949
2.2	-64074	-173058	-173890	-181509	-201590	-237259	-265725	-287890	-301764
2.3	-56978	-154013	-154748	-161439	-178603	-209352	-233754	-252854	-265216
2.4	-50072	-134694	-135611	-141081	-155689	-181824	-202628	-218861	-229496
2.5	-43497	-116228	-116613	-121666	-133372	-155784	-172944	-186684	-195217
$R_G = 22 h^{-1} \text{Mpc}$									
-2.5	-12844	-13354	-13600	-15337	-16780	-16807	-15401	-14119	-12612
-2.4	-14854	-15431	-15829	-17695	-19430	-19342	-17876	-16288	-14565
-2.3	-16849	-17484	-17942	-20206	-22028	-21906	-20329	-18395	-16472
-2.2	-18856	-19555	-20054	-22606	-24555	-24530	-22562	-20374	-18214
-2.1	-20729	-21610	-22013	-24734	-26864	-26714	-24672	-22257	-19815
-2.0	-22274	-23239	-23658	-26660	-28919	-28559	-26452	-23712	-21042
-1.9	-23563	-24606	-25002	-27868	-30160	-29912	-27449	-24744	-21776
-1.8	-24383	-25300	-25774	-28504	-30899	-30523	-27934	-24806	-21744
-1.7	-24319	-25472	-25911	-28327	-30678	-30175	-27275	-24114	-20875
-1.6	-23552	-24593	-25113	-27332	-29345	-28587	-25878	-22394	-19078
-1.5	-22029	-22755	-23265	-25192	-26906	-26048	-23201	-19523	-16178
-1.4	-19384	-20257	-20447	-21838	-23265	-22006	-18939	-15378	-12329
-1.3	-15861	-16287	-16520	-17431	-18081	-16472	-13409	-9740	-7148
-1.2	-11143	-11287	-11737	-11725	-11464	-9641	-6630	-2985	-480
-1.1	-5672	-5504	-5528	-4882	-3675	-1452	1517	5031	7150
-1.0	798	975	1243	2797	4987	7608	10663	14062	15805
-0.9	7885	8342	8691	10976	14479	17511	20559	23967	25243
-0.8	15496	16038	16749	19943	24403	27965	30638	33980	34978
-0.7	22911	23809	24935	29156	34474	38313	40732	44244	44712
-0.6	30511	31933	33051	38183	44454	48555	50774	53895	54360
-0.5	37709	39351	40376	46529	53505	57923	60067	63004	63186
-0.4	44138	45966	47240	53677	61224	65991	68138	70686	70306
-0.3	49717	51460	52750	59485	67650	72718	74317	76483	75982

Table 7—Continued

$\nu$	$\bar{d}/R_G = 0.08$	0.16	0.32	0.64	1.0	$\sqrt{2}$	$\sqrt{3}$	2.0	$\sqrt{5}$
-0.2	53569	55728	56774	63845	72250	77222	78558	79944	80001
-0.1	56079	58040	59463	66086	74762	79241	80715	81341	82071
0.0	56748	58696	60024	66780	75083	79270	80382	80680	81265
0.1	55917	57799	58750	65380	72879	77103	77705	77567	78072
0.2	53226	55093	55930	61973	68813	72300	72770	71943	72383
0.3	49125	50490	51493	56736	63083	65625	65741	64824	64486
0.4	43441	44502	45616	49795	55189	56828	56840	55703	54977
0.5	36605	37709	38545	42081	45846	47180	46378	45179	44267
0.6	29505	30192	30702	33329	35881	36448	35171	33950	32573
0.7	21717	22272	22466	24126	25489	25147	23655	22115	20591
0.8	13793	14235	14180	14782	15164	13895	12239	10780	8782
0.9	5987	6218	6056	5667	5072	3100	1230	-318	-2268
1.0	-1291	-1401	-1722	-2848	-4273	-7017	-8777	-10499	-12437
1.1	-7738	-8162	-8390	-10444	-12805	-16029	-17850	-19454	-21313
1.2	-13389	-13960	-14285	-16936	-20202	-23410	-25605	-27246	-28571
1.3	-18018	-18639	-19267	-22124	-26016	-29747	-31646	-33377	-34223
1.4	-21607	-22290	-23003	-26024	-30662	-34246	-36180	-37769	-38628
1.5	-24030	-24923	-25469	-28788	-33533	-37203	-39110	-40538	-41639
1.6	-25565	-26425	-26931	-30303	-35316	-38944	-40786	-42049	-42804
1.7	-26322	-26969	-27596	-30870	-35865	-39253	-41329	-42400	-42921
1.8	-26092	-26771	-27300	-30504	-35319	-38599	-40292	-41483	-42070
1.9	-25182	-25903	-26386	-29434	-34071	-37024	-38520	-39493	-39948
2.0	-23804	-24471	-24849	-27742	-31838	-34712	-36128	-36930	-37405
2.1	-22021	-22450	-23008	-25534	-29360	-31972	-33090	-33809	-34229
2.2	-19907	-20408	-20922	-23249	-26563	-28807	-29757	-30457	-30751
2.3	-17707	-18202	-18678	-20717	-23673	-25566	-26288	-26911	-27347
2.4	-15613	-16077	-16455	-18181	-20679	-22445	-22866	-23527	-23790
2.5	-13536	-13970	-14218	-15665	-17856	-19326	-19668	-20186	-20380

Note. — Genus values at a given threshold level of the density field estimated from randomly sampled simulation particles to have mean particle separations of  $\bar{d}/R = 0.08, 0.16, 0.32, 0.64, 1.0, \sqrt{2}, \sqrt{3}, 2.0, \sqrt{5}$  using the smallest possible pixel size ( $2160^3$  in this case).

Table 8. Genus Values at a Given Threshold Level for the Samples to Estimate the Effects of Shot Noise in the Halo Density Field

$\nu$	$\bar{d}/R_G = 1.0$	$\sqrt{2}$	$\sqrt{3}$	2.0	$\sqrt{5}$
$R_G = 15 \ h^{-1}\text{Mpc}$					
-2.5	-102261	-108020	-109474	-106170	-101833
-2.4	-117627	-123827	-125504	-121650	-116447
-2.3	-132824	-139315	-140723	-137159	-130756
-2.2	-147195	-154361	-155424	-151801	-144163
-2.1	-160452	-167495	-168485	-163702	-155013
-2.0	-170947	-177252	-177619	-172557	-162893
-1.9	-177276	-182981	-182718	-176658	-166152
-1.8	-179216	-182780	-182135	-175039	-163838
-1.7	-174754	-176636	-174517	-166667	-154063
-1.6	-163768	-162520	-158629	-149564	-136685
-1.5	-145480	-140541	-133559	-123369	-110014
-1.4	-118359	-109849	-100048	-87422	-73636
-1.3	-83337	-70361	-56574	-42703	-26844
-1.2	-39293	-22161	-4746	12335	29660
-1.1	10781	33457	55363	75117	94038
-1.0	67923	95597	121050	143155	162763
-0.9	129579	161808	190883	215662	236596
-0.8	194007	230086	262897	289390	310610
-0.7	258434	297029	331883	361392	382265
-0.6	319970	360435	397567	427809	447209
-0.5	375748	418230	455066	484099	504355
-0.4	423008	465165	501746	530790	549739
-0.3	459398	501054	534786	562431	579517
-0.2	484631	522542	553703	578904	592422
-0.1	495940	528805	555779	576657	588063
0.0	492597	518380	540967	556871	564573
0.1	473891	492472	509659	520117	523738
0.2	441327	451759	462218	466762	466319
0.3	394982	398062	402301	399666	395809
0.4	340326	333713	329257	322895	315912
0.5	277462	260998	248828	237276	227391
0.6	208490	183080	164819	148803	135606
0.7	136121	103644	79499	59913	44572
0.8	64902	25544	-3520	-26164	-42887
0.9	-3867	-47742	-80447	-105376	-123637
1.0	-66799	-115078	-150026	-175245	-194174
1.1	-122715	-173527	-209089	-234217	-253666
1.2	-170334	-221263	-257194	-282181	-299266
1.3	-207441	-258785	-293146	-316599	-331726
1.4	-235223	-285054	-317405	-338436	-351558
1.5	-252821	-300189	-329796	-348415	-359032
1.6	-261786	-305509	-331616	-347459	-355659
1.7	-262781	-302178	-324510	-336669	-343502
1.8	-256944	-291340	-309915	-319156	-323581
1.9	-245387	-275040	-289673	-296387	-298510
2.0	-228725	-254128	-265647	-269897	-269677
2.1	-209709	-230806	-238976	-241136	-239522
2.2	-188317	-205504	-211144	-211829	-209157
2.3	-166473	-180325	-183664	-182938	-179760
2.4	-144722	-155422	-156655	-155250	-151999
2.5	-124021	-132169	-131975	-129767	-126670
$R_G = 22 \ h^{-1}\text{Mpc}$					
-2.5	-39240	-41259	-41109	-39327	-36984
-2.4	-45125	-47043	-47054	-45075	-42217
-2.3	-50919	-53069	-52780	-50953	-47455
-2.2	-56411	-58272	-58466	-55967	-52223
-2.1	-61145	-63374	-63524	-60588	-56409
-2.0	-64882	-67341	-67200	-64109	-59086
-1.9	-67059	-69271	-69026	-65674	-60484
-1.8	-67728	-69454	-68577	-64794	-59760
-1.7	-65966	-67060	-65555	-61641	-56524
-1.6	-61641	-62013	-60027	-55782	-50435



Table 8—Continued

$\nu$	$\bar{d}/R_G = 1.0$	$\sqrt{2}$	$\sqrt{3}$	2.0	$\sqrt{5}$
-1.5	-54512	-53243	-50637	-46547	-40904
-1.4	-44231	-41785	-37999	-33344	-27912
-1.3	-30665	-26945	-22160	-16933	-11368
-1.2	-14141	-8767	-2800	3178	8265
-1.1	5592	12530	19153	26188	31360
-1.0	27243	36448	43587	51207	56317
-0.9	50801	61563	69836	78177	83189
-0.8	75305	87308	96906	105178	110616
-0.7	99154	112420	122738	131487	136867
-0.6	121886	136108	147130	155495	160938
-0.5	142869	157547	168344	176823	181592
-0.4	160525	174935	185602	192945	198259
-0.3	174053	188207	197883	204058	209079
-0.2	182765	196347	204596	210383	214219
-0.1	186476	197740	206139	210769	213430
0.0	184577	193817	200893	203528	205155
0.1	177239	183928	189136	190869	190938
0.2	164478	168156	171139	171460	170946
0.3	146916	147916	148645	147412	146002
0.4	125546	123652	122374	119459	116617
0.5	101133	96432	93219	88841	84891
0.6	74849	67364	62297	56920	51770
0.7	47330	37850	30330	24670	18811
0.8	20326	9308	-124	-6147	-12533
0.9	-5355	-18105	-28083	-34906	-41649
1.0	-28645	-42811	-53679	-60894	-67294
1.1	-49424	-64795	-75767	-83063	-88872
1.2	-67092	-82611	-93669	-100550	-106199
1.3	-80908	-96550	-107076	-113841	-118475
1.4	-90900	-106081	-116170	-122405	-126265
1.5	-97174	-111921	-121026	-126528	-129264
1.6	100085	-113943	-122360	-126783	-128716
1.7	100080	-113051	-120183	-123460	-124694
1.8	-97305	-108877	-115058	-117521	-118152
1.9	-92841	-102527	-107607	-109793	-109814
2.0	-86288	-94916	-98579	-100293	-99993
2.1	-78719	-86262	-88788	-89855	-89278
2.2	-70751	-76817	-78635	-79231	-78175
2.3	-62751	-67658	-68476	-68528	-67542
2.4	-54656	-58547	-58758	-58571	-57427
2.5	-46823	-49771	-49782	-49169	-48194

$R_G = 34 h^{-1} \text{Mpc}$					
$\nu$	$\bar{d}/R_G = 1.0$	$\sqrt{2}$	$\sqrt{3}$	2.0	$\sqrt{5}$
-2.5	-13003	-13331	-13040	-12410	-11284
-2.4	-14855	-15434	-14949	-14116	-12996
-2.3	-16752	-17358	-16779	-15922	-14629
-2.2	-18574	-19165	-18415	-17569	-16130
-2.1	-20149	-20684	-20014	-19069	-17350
-2.0	-21432	-21861	-21380	-20081	-18322
-1.9	-22160	-22729	-22002	-20662	-18817
-1.8	-22333	-22850	-22062	-20632	-18437
-1.7	-21698	-22082	-21461	-19603	-17600
-1.6	-20253	-20407	-19827	-17937	-15661
-1.5	-17983	-17881	-17046	-15132	-12864
-1.4	-14680	-14215	-13249	-11211	-9000
-1.3	-10304	-9514	-8122	-5975	-4365
-1.2	-5102	-3738	-2146	142	1631
-1.1	1005	2955	4921	7094	8514
-1.0	8260	10405	12707	14570	15996
-0.9	15829	18394	20947	22775	23935
-0.8	23590	26694	29452	31074	32053
-0.7	31563	34943	37767	39350	40216
-0.6	38994	42745	45582	46744	47957
-0.5	45453	49689	52267	53517	54663
-0.4	51101	55463	58003	58984	59819
-0.3	55801	59482	62087	62933	63356

## REFERENCES

- Adler, R. J. 1981, *The Geometry of Random Fields* (New York, Wiley)
- Blake, C., Berian, J. J., & Poole, G. B. 2013, *MNRAS*, in press
- Choi, Y.-Y., Park, C., Kim, J., et al. 2010, *ApJS*, 190, 181
- Choi, Y.-Y., Kim, J., Rossi, G., et al. 2013, *ApJS*, 209, 19
- Doroshkevich, G. 1970, *Astrophysika*, 6, 320
- Gott, J. R., Melott, A. L., & Dickinson, M. 1986, *ApJ*, 306, 341
- Gott, J. R., et al. 1989, *ApJ*, 340, 625
- Gott, J. R., Choi, Y.-Y., Park, C., & Kim, J. 2009, *ApJ*, 695, L45
- Hamilton, A. J. S., Gott, J. R., & Weinberg, D. W. 1986, *ApJ*, 309, 1
- Hikage, C., Schmalzing, J., Buchert, T., Suto, Y., Kayo, I., Taruya, A., Vogeley, M. S., Hoyle, F., Gott, J. R., & Brinkmann, J. 2003, *PASJ*, 55, 911
- Hikage, C., Komatsu, E., & Matsubara, T. 2006, *ApJ*, 653, 11
- Hikage, C., Coles, P., Grossi, M., Moscardini, et al. 2008, *MNRAS*, 385, 1613
- Hockney, R. W., & Eastwood, J. W. 1981, *Computer Simulations Using Particles*, McGraw-Hill, New York
- James, J. B. 2012, *ApJ*, 751, 40
- Jee, I., Park, C., Kim, J., Choi, Y.-Y., & Kim, S. S. 2012, *ApJ*, 753, 11
- Kim, J., & Park, C. 2006, *ApJ*, 639, 600
- Kim, J., Park, C., & Choi, Y.-Y. 2008, *ApJ*, 683, 123
- Kim, J., Park, C., Gott, J. R., & Dubinski, J. 2009, *ApJ*, 701, 1547
- Kim, J., Park, C., Rossi, G., Lee, S. M., & Gott, J. R. 2011, *JKAS*, 44, 217
- Komatsu, E., Dunkley, J., Nolta, M. R., et al. 2009 *ApJS*, 180, 300
- L’Huiller, B., Park C., & Kim, J. 2014, *New Astronomy*, submitted
- Matsubara, T. 1994, *ApJ*, 434, L43

Table 8—Continued

$\nu$	$\bar{d}/R_G = 1.0$	$\sqrt{2}$	$\sqrt{3}$	2.0	$\sqrt{5}$
-0.2	58512	62199	64391	65077	65149
-0.1	59865	62805	64698	65070	65130
0.0	59107	61839	63414	63010	62845
0.1	56758	58983	60065	59689	59187
0.2	52722	54259	54662	54115	53504
0.3	46948	48247	47700	47126	45825
0.4	39850	40422	39422	38493	37268
0.5	32045	31724	30358	29220	27764
0.6	23701	22500	20633	19506	17914
0.7	14891	13017	10983	9542	7968
0.8	6462	3769	1554	145	-1783
0.9	-1960	-4709	-7158	-9108	-11023
1.0	-9337	-12696	-15386	-16972	-18989
1.1	-15834	-19590	-22466	-24032	-25592
1.2	-21350	-25204	-28120	-29663	-31254
1.3	-25789	-29683	-32332	-33969	-35262
1.4	-28871	-32838	-35265	-36716	-37851
1.5	-31018	-34746	-37004	-38158	-39063
1.6	-31873	-35456	-37565	-38514	-39273
1.7	-31775	-35277	-37080	-37839	-38406
1.8	-31079	-33946	-35419	-36344	-36496
1.9	-29580	-32029	-33483	-34103	-34085
2.0	-27555	-29677	-30998	-31259	-31187
2.1	-25177	-26956	-28029	-28243	-28017
2.2	-22541	-24151	-24925	-24974	-24821
2.3	-19915	-21277	-21783	-21754	-21564
2.4	-17405	-18449	-18679	-18714	-18456
2.5	-14957	-15679	-15821	-15895	-15487

Note. — Genus values at a given threshold level of the halo density field estimated from randomly selected halos to have mean halo separations of  $\bar{d}/R = 1.0, \sqrt{2}, \sqrt{3}, 2.0, \sqrt{5}$  using the smallest possible pixel size ( $2160^3$  in this case).

- Matsubara, T. 1996, *ApJ*, 457, 13
- Matsubara, T., & Suto, Y. 1996, *ApJ*, 460, 51
- Matsubara, T. 2003, *ApJ*, 584, 1
- Mecke, K. R., Buchert, T., & Wagner, H. 1994, *A&A*, 288, 697
- Melott, A. L., Weinberg, D. H., & Gott, J. R. 1988, *ApJ*, 328, 50
- Melott, A. L., Cohen, A. P., Hamilton, A. J. S., Gott, J. R., & Weinberg, D. H. 1989, *ApJ*, 345, 618
- Melott, A. L., & Dominik, K. G. 1993, *ApJS*, 86, 1
- Neyrinck, M. C., Szapudi, I., & Szalay, A. S. 2011, *ApJ*, 731, 116
- Park, C., & Gott, J. R. 1991, *ApJ*, 378, 457
- Park, C., Kim, J., & Gott, J. R. 2005, *ApJ*, 633, 1
- Park, C., & Kim, Y.-R. 2010, *ApJ*, 715, L185
- Park, C., Pranav, P., Chingangbam, P., van de Weygaert, R., Jones, B., Vegter, G., Kim, I., Hidding, J., & Hellwing, W. A. 2013, *JKAS*, 46, 125
- Prattern, G., & Munchi, D. 2012, *MNRAS*, 423, 3209
- Speare, R., Gott, J. R., Kim, J., & Park, C. 2013, arXiv1310.4278
- Tomita, H. 1986, *Progress of Theoretical Physics*, 76, 952
- Verde, L., et al. 2003, *ApJS*, 148, 195
- Vogeley, M. S., Park, C., Geller, M. J., Huchra, J. P., & Gott, J. R. 1994, *ApJ*, 420, 525
- Wang, X., Xuelei, C., & Park, C. 2012, *ApJ*, 747, 48
- Way, M. J., Gazis, P. R., & Scargle, J. D. 2011, *ApJ*, 727, 48
- Weinberg, D. H., Gott, J. R., & Melott, A. L. 1987, *ApJ*, 321, 2
- Weinberg, D. H., & Cole, S. 1992, *MNRAS*, 259, 652
- Zunckel, C., Gott, J. R., & Lunnan, R. 2011, *MNRAS*, 412, 1401